Dissertation zur Erlangung des Doktorgrades
an der Fakultät für Chemie und Pharmazie
der Ludwig-Maximilians-Universität München

Characterization of the myxobacterial compound Chondramide as novel anti-angiogenic and anti-metastatic agent

Magdalena Helga Menhofer

aus Landshut

2014

Erklärung

Diese Dissertation wurde im Sinne von §7 der Promotionsordnung vom 28. November 2011 von Herrn Prof. Dr. Stefan Zahler betreut.

Eidesstattliche Versicherung

Diese Dissertation wurde eigenständig und ohne unerlaubte Hilfe erarbeitet.

München, den 04. Februar 2014

Magdalena Helga Menhofer

Dissertation eingereicht am: 06. Februar 2014

1. Gutachter:	Herr Prof. Dr. Stefan Zahler
2. Gutachterin:	Frau Prof. Dr. Angelika M. Vollmar
Mündliche Prüfung am:	14. März 2014

Meinen Eltern und Geschwistern

Contents

1 Introduction **1**

1.1 Chemotherapy targeting the cytoskeleton . . . 1
1.2 Actin as a potential target . . . 1
1.2.1 Advantages of actin targeting . . . 1
1.2.2 Actin structures and their cellular function . . . 2
1.3 Source for actin targeting: natural compounds . . . 4
1.4 Myxobacteria as pharmaceutical factory . . . 4
1.5 Chondramide . . . 5
1.5.1 Isolation and structure of Chondramide . . . 5
1.5.2 First cellular studies with Chondramide . . . 5
1.6 Actin dependent processes in the progression of cancer . . . 6
1.6.1 Angiogenesis . . . 6
1.6.2 Metastasis . . . 7
1.6.3 Cell migration . . . 7
1.6.4 Signaling regulating actin in cell migration . . . 9
1.7 Aim of the study . . . 12

2 Material and Methods **14**

2.1 Materials . . . 14
2.1.1 Compounds . . . 14
2.1.2 Reagents, dyes and inhibitors . . . 14
2.2 Cell culture . . . 16
2.2.1 Solutions and reagents . . . 16
2.2.2 Endothelial cells . . . 16
2.2.3 Cancer cells . . . 17
2.2.4 Passaging . . . 18
2.2.5 Freezing and thawing . . . 18
2.3 Angiogenesis assays . . . 18
2.3.1 Proliferation assay . . . 18
2.3.2 Scratch assay . . . 19
2.3.3 Chemotaxis assay . . . 19
2.3.4 Tube formation assay . . . 19
2.3.5 Adhesion assay . . . 19
2.4 Metastasis assays . . . 20

2.4.1 Scratch assay . . . 20
2.4.2 Boyden chamber assay . . . 20
2.4.3 Invasion assay . . . 20
2.4.4 Adhesion assay . . . 21
2.5 Flow cytometry (FACS) . . . 21
2.5.1 Measurement of sub-diploid DNA content . . . 21
2.5.2 Measurement of membraneous, extracellular proteins . . . 21
2.6 Propidium iodide staining for microscopy . . . 22
2.7 Transfection of cells . . . 22
2.8 Microscopy . . . 23
2.8.1 Microscopy with fixed cells . . . 23
2.8.2 Life cell imaging . . . 24
2.8.3 Histological stainings . . . 24
2.9 Measurement of cellular contractility . . . 25
2.9.1 Contractility assay . . . 25
2.9.2 Image processing . . . 26
2.9.3 PIV analysis . . . 26
2.10 Western blot analysis . . . 27
2.11 Pull down assay . . . 29
2.12 Statistical analysis . . . 29

3 Results **30**
3.1 Chondramide diminishes angiogenesis *in vitro* and *in vivo* . . . 30
3.1.1 Chondramide inhibits proliferation of endothelial cells at nanomolar concentrations . . . 30
3.1.2 Chondramide diminishes endothelial cell migration but not specifically chemotaxis . . . 31
3.1.3 Chondramide disrupts tube formation in a concentration and time dependent manner . . . 33
3.1.4 Chondramide leads to actin aggregation forming aggresomes . . . 35
3.1.5 Chondramide reduces adhesion on collagen and the maturation of focal adhesions . . . 39
3.1.6 Chondramide affects integrin associated signaling by inhibiting Src activity . . . 41
3.1.7 Chondramide reduces Rho GTPase activity . . . 44
3.1.8 Chondramide diminishes angiogenesis *in vivo* . . . 46
3.2 Chondramide inhibits metastasis *in vitro* and *in vivo* . . . 47
3.2.1 Chondramide diminishes metastasis *in vivo* . . . 47
3.2.2 Chondramide reduces migration of highly invasive cancer cells . . . 49
3.2.3 Chondramide inhibits FCS induced migration and invasion *in vitro* . . . 50
3.2.4 Chondramide reduces adhesion of MDA-MB-231 cells on several surfaces . . . 51
3.2.5 Chondramide affects stress fibers of MDA-MB-231 cells . . . 52

3.2.6 Chondramide reduces the activity of the RhoGTPase Rho but not Rac1 52
3.2.7 Chondramide has no effect on the activation of the EGF-receptor and downstream signaling . . . 54
3.2.8 Chondramide diminishes cellular contractility . . . 56

4 Discussion **58**
4.1 Chondramide as anti-angiogenic agent . . . 58
4.1.1 Actin targeting in anti-angiogenic therapy . . . 58
4.1.2 Chondramide induces aggresome formation . . . 59
4.1.3 Chondramide reduces stress fibers potentially diminishing focal adhesion maturation . . . 59
4.1.4 Chondramide diminishes signal transduction at focal adhesions and downstream signaling . . . 60
4.1.5 Conclusion concerning angiogenesis . . . 61
4.2 Chondramide as anti-metastatic compound . . . 62
4.2.1 Chondramide impairs cellular contractility in amoeboid cell migration 62
4.2.2 Chondramide impairs pro-contractile signaling . . . 63
4.2.3 Chondramide shows anti-metastatic effects without acute toxicity . . . 63
4.2.4 Conclusion concerning metastasis . . . 64
4.3 Chondramide as a dual inhibitor of angiogenesis and metastasis . . . 64
4.4 Future perspectives . . . 65
4.4.1 Treatment of anti-angiogenic resistant tumors . . . 65
4.4.2 Targeting both invasive migration modes to inhibit metastasis . . . 66
4.4.3 Improvement of tissue selectivity . . . 66

5 Summary **67**

Literature **69**

Appendix **77**
6.1 Abbreviations . . . 77
6.2 Publications . . . 78
6.2.1 Articles . . . 78
6.2.2 Oral presentations . . . 78
6.2.3 Poster presentations . . . 79
6.3 Danksagung . . . 80

1: Introduction

1.1 Chemotherapy targeting the cytoskeleton

Since decades, the cytoskeleton is targeted in the chemotherapeutic treatment of cancer. Drugs targeting microtubules have been used in the clinic since the early 60s and are the most frequently applied class of anti cancer drugs [1, 2]. The functionality of microtubule targeting drugs is attributed to the inhibition of mitosis as well as the induction of apoptosis, inhibition of angiogenesis and metastasis [3, 2]. Although a very ubiquitous protein is targeted, the widespread use in the clinic reflects the pharmacological importance of microtubule targeting drugs. However, side effects affecting the nervous system and the development of resistances constantly raise the need for new targets and strategies. Analogue to microtubules, the cytoskeletal component actin is involved in pro-oncogenic processes like cytokinesis as well as angiogenesis and metastasis. These parallels highlight the actin cytoskeleton as an interesting target for cancer therapy.

1.2 Actin as a potential target

1.2.1 Advantages of actin targeting

Actin reveals several advantages as a target in cancer therapy. First of all, actin is the most abundant protein through all eukaryotes and even bacteria show derivatives [4, 5, 6]. Through all those species, the structure of actin is highly conserved and actin interacts with more than 100 other proteins requiring a stringent conserved structure. Due to this enormous conservation, actin is very unlikely to mutate and develop resistances against therapies. Second, cancer cells reveal differences in actin turnover compared to normal cells. So

cancer cells show a higher value of unpolymerized actin compared to normal cells [7] and during metastasis a higher actin turnover is required than for stationary cells which could make them more vulnerable to actin binding substances compared to normal tissue. Third, the more aggressive mesenchymal cells are more sensitive to actin targeting compounds whereas more quiescent, epithelial like cells show higher sensitivity to microtubule binding agents [8] revealing actin as the preferable target for mesenchymal cells.
Despite all these advantages, actin itself was not considered as a potential target during the last decades. The reason therefore lies mostly in the very first *in vivo* studies. In 1985 the actin binding compound Phalloidin was administered *in vivo* and referred to be too toxic due to liver toxicity [9]. 1988, Scott and collegues tested Jasplakinolide *in vivo* and proposed the subastance as too toxic for clinical application [10]. However, new actin binding substances with modified properties are still found and the combination with modern targeting strategies could facilitate their use nowadays.

1.2.2 Actin structures and their cellular function

Structurally, the actin molecule is a 42 kDa, globular protein that forms microfilaments. Actin monomers (G-actin) spontaneously polymerize into linear filaments (F-actin) with a minimal nucleation seed of four monomers. Actin filaments are directed as all monomers are oriented in the same direction leading to a so called barbed and a pointed end whereby polymerization occurs predominantly at the barbed end (Figure 1.1 A). Actin polymers are further processed via a high number of actin interacting proteins. So the polymerization of actin is enhanced by the nucleation and elongation factor Formin. Existing filaments are prevented from elongation e.g. by the barbed-end capping protein CapZ or can be refracted by severing proteins like Gelsolin or Cofilin. Further, net like structures are facilitated by Arp2/3 complex binding to existing filaments enabling the nucleation of new filaments in an angle of 70° (Figure 1.1 B). The concerted action of all these proteins transforms linear actin polymers in more complex structures, as there are: the contractile ring, lamellipodia or stress fibers (Figure 1.1 C). These higher structures finally fulfill the actin dependent cellular functions like cytokinesis, cellular protrusion and cellular contractility, respectively. [4, 11]

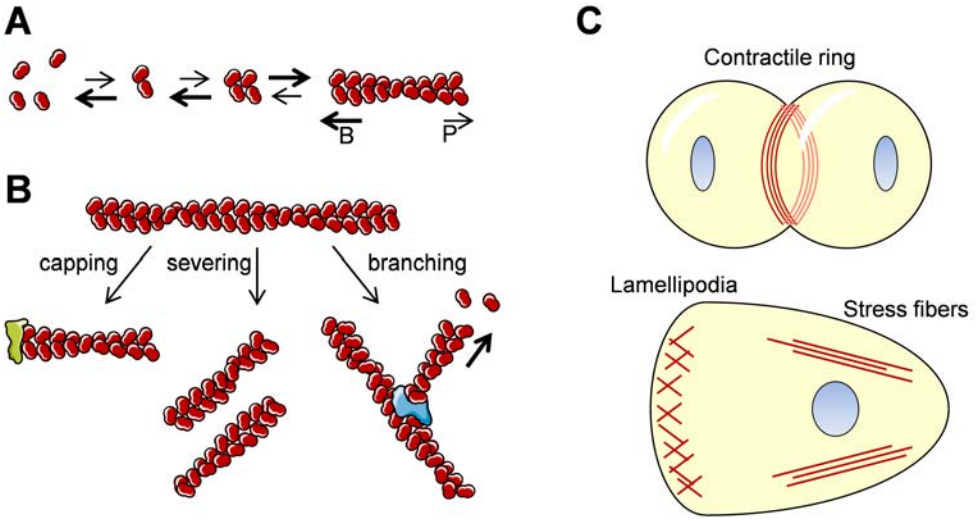

Figure 1.1: **Actin structures.** A: Polymerization of actin. Actin polymerization requires a minimum of four subunits for efficient polymerization. Polymerization is faster at the barbed end (B) compared to the pointed end (P). B: Complex actin structures are achieved by the interaction with actin binding proteins leading to capping, severing or branching of actin fibers. C: Actin builds up the contractile ring in cytokinesis as well as lamellipodia and stress fibers in migrating cells.

1.3 Source for actin targeting: natural compounds

Many chemotherapeutics were inspired by compounds isolated from natural sources [12, 13]. In case of microtubules, even all therapeutically applied tubulin binding drugs are natural compounds or derivatives [2]. Interestingly, also for actin, nature has developed several compounds binding and affecting actin filaments [14, 15]. So obviously, also nature has regarded the actin cytoskeleton as a rewarding target.

The actin binding compounds can be distinguished in two groups: first, F-actin stabilizing and, second, F-actin destabilizing compounds. The most well known agents as F-actin stabilizer are Phalloidin which was first isolated from 'Death cap' mushroom *Amanita phalloides* and Jasplakinolide from the marine sponge *Jaspis johnstoni* [16, 17]. As F-actin destabilizer Cytochalasins, from fungea, and Latrunculin A from the Red Sea sponge *Negombata magnifica* [18, 19] are the most prominent representatives. Further, the list can be elongated as new compounds are still found.

1.4 Myxobacteria as pharmaceutical factory

An enormous source of pharmaceutically active compounds are myxobacteria. Myxobacteria belong to proteobacteria, reside mainly in soil [20, 21] and are characterized by the formation of fruiting bodies when resources are rare [20]. For pharmacological development, myxobacteria are attractive due to their rich metabolomic diversity enabling them to produce a huge number of secondary metabolites structurally different from those from other microbes [22, 23]. In fact, 40% of the myxobacterial compounds include novel chemical structures [20]. Additionally, recent developments in the cultivation of myxobacteria and the possibility of genetic engineering will further increase the possiblities for the identification and production of pharmacologically active compounds.

1.5 Chondramide

1.5.1 Isolation and structure of Chondramide

Among the myxobacterial compounds is the group of actin binding agents, the Chondramides, originally isolated from myxobacterium *Chondromyces crocatus* [24]. Structurally, they are C-18 cyclodepsipeptides consisting of a tripeptide with Ala-Trp-Tyr-sequence closed to a circle via a polyketide (Figure 1.2). The major derivatives are Chondramide A-D that differ in a methoxylation at the ring or a chloration at the Tyr side chain (Figure 1.2) [25, 24].

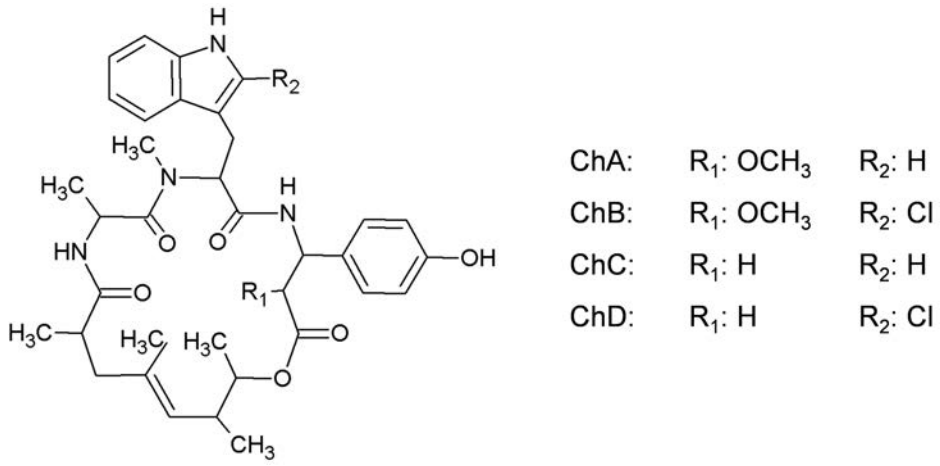

Figure 1.2: **Chemical structure of Chondramide A to D**

1.5.2 First cellular studies with Chondramide

So far, it is known that Chondramides bind actin competitively to Phalloidin and accelerate actin polymerization in pyrene assay [26]. On a cellular level, Chondramides inhibit proliferation of cancer cells, induce actin lumps [26] and fluorescently labeled Chondramide preferably binds stress fibers [27]. However, detailed mechanisms on anti-cancer activity are unknown.

1.6 Actin dependent processes in the progression of cancer

During tumor development, actin plasticity is highly required in angiogenesis and metastasis revealing those as interesting processes to target.

1.6.1 Angiogenesis

Angiogenesis is defined as the formation of new blood vessels from already existing ones. This formation of new vessels is involved in natural processes like reproduction, development and wound repair, as well as pathological processes such as autoimmune diseases, age-related macular degeneration, atherosclerosis and cancer [28]. In all non-malignant processes, a balance of pro- and anti-angiogenic signals keeps the endothelium quiescent. However, in cancer tissue insufficient supply of nutrients causes an elevated release of pro-angiogenic factors. Those factors, like for example the vascular endothelial growth factor (VEGF) stimulate quiescent endothelial cells starting the angiogenic cascade (Figure 1.3). Thereby, endothelial cells get activated and start to proliferate. Extracellular matrix (ECM) becomes degraded and endothelial cells migrate towards a chemotactic gradient. From those, tubes are formed and, finally, the established vasculature gets stabilized. [29]

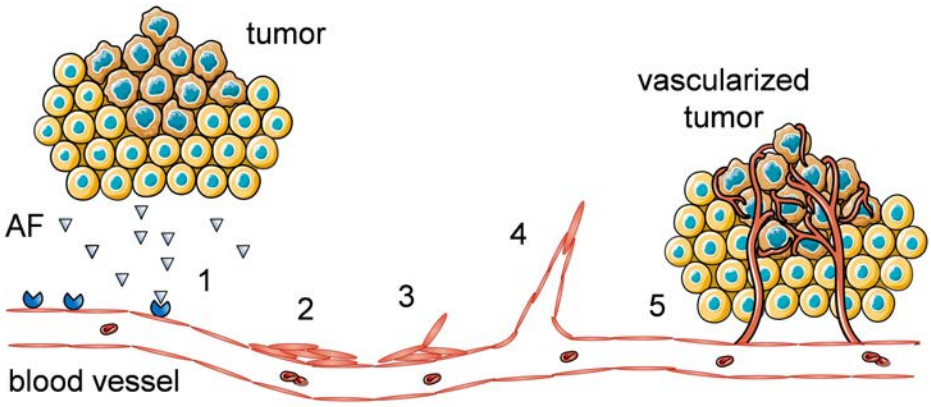

Figure 1.3: **The angiogenic cascade.** In the process of angiogenesis, angiogenic factors (AF) stimulate quiescent endothelial cells (1), which start to proliferate (2), to degrade extracellular matrix and migrate along the chemotactic gradient (3). Endothelial cells form tubes (4), which, finally, get stabilized and supply the tumor with nutrients and oxygen (5).

1.6.2 Metastasis

In case of insufficient angiogenesis or the supply of nutrients, cancer cells are able to transform to a motile phenotype and invade the tumor surrounding tissue initiating metastasis. After the first transformation and the local invasion, metastizing cells intravasate into blood vessels. In those, cells need to survive in the circulation and, finally, get trapped in capillaries, e.g. in the lung or liver. Here, tumor cells adhere and extravasate from the vessel to invade the surrounding tissue. Within the new host tissue, cells need to adapt and proliferate to form new colonies, named metastasis. All these steps are necessary for the development of metastasis and each can be rate limiting or stop the whole process (Figure 1.4). [30, 31]

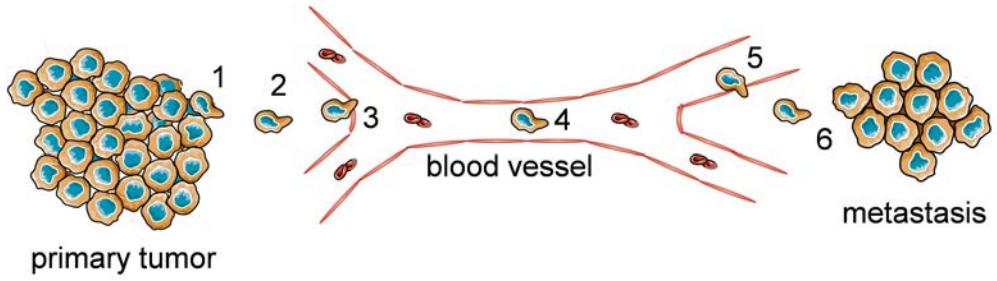

Figure 1.4: **The metastatic cascade.** For the development of metastasis, cancer cells need to acquire invasive properties (1), invade normal tissue (2), intravasate into blood vessels (3), survive during circulation (4), adhere and extravasate (5) and, finally, adapt and proliferate in new tissues (6).

1.6.3 Cell migration

In angiogenesis as well as metastasis the migration of endothelial or cancer cells, respectively, is a major step contributing to the progression of cancer. Cellular migration is a repetitive process of five major steps [32, 33]. First, cells sense chemotactic stimuli, protrude in that direction, attach to new surfaces, contract the rear in the direction of migration and, finally, release adhesions at the rear to proceed (Figure 1.5 A). In all these processes, the actin cytoskeleton represents the major structure determining element. Sensing is mediated by filopodia which are thin long fingerlike membrane protrusions mediated by long parallel actin bundles (Figure 1.5 A, B). Second, cellular protrusion is accomplished via lamellipodia, a 2 μm thick, dense actin-network at the leading edge pushing the membrane into the

direction of migration. And third, cellular contraction is facilitated by thick actin strands throughout the cell body called stress fibers. Those stress fibers end up at sites of adhesion interacting with the assembly and disassembly of the adhesive structures called focal adhesions. [32, 34]

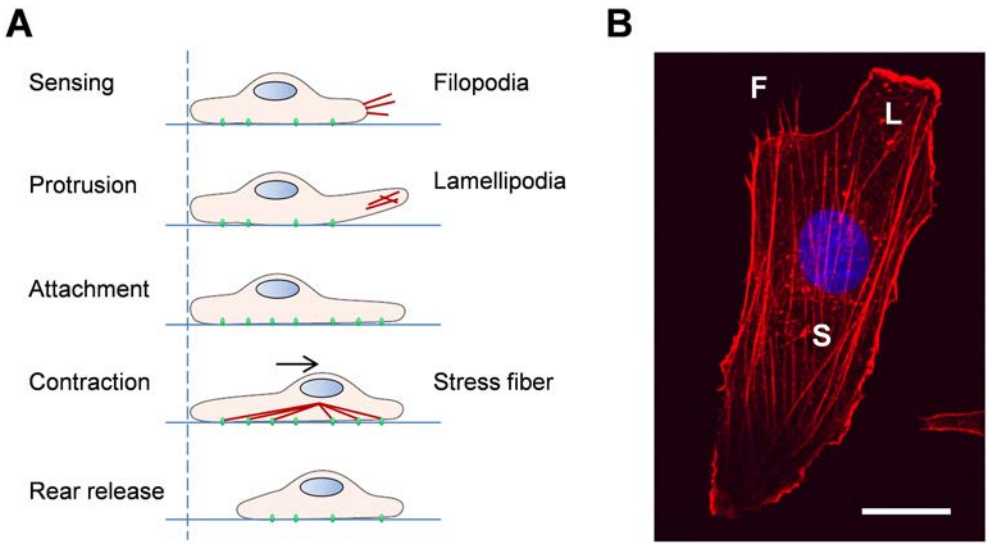

Figure 1.5: **Cellular migration.** A: Illustration of the five steps within a migratory cycle. Actin structures are displayed in red, focal adhesions in green and the nucleus in blue. B: Actin staining of HMEC-1 showing the most representative actin structures (red): F: filopodia, L: lamellipodia, S: stress fibers. Bar represents 20 μm.

For metastatic cells, additional migration modes are described in 3D environment. Invasive cells show two modes of migration in 3D: first, the mesenchymal type and, second, the amoeboid type of migration [35, 36, 37]. In the mesenchymal migration, cells show an elongated morphology with lamellipodial protrusions and high proteolytic activity. Contrarily, the amoeboid migration mode is totally independent of proteolysis and can be induced as an escape mode when proteolysis is inhibited. In this migration type, cells show rounded shape and invasion through the matrix is only mediated via cellular contractility. The underlying signaling pathway involves Rho/ROCK and myosin to induce the actin dependent contractile force which will be explained in the next paragraph. In both processes, the actin cytoskeleton plays a central role either for the formation of protrusions or the contraction of the cell. Therefore, the actin machinery represents an attractive target to address metastatic cells.

1.6.4 Signaling regulating actin in cell migration

The formation of actin structures is highly regulated. Chemotactic, haptotactic or mechanic stimuli are transmitted to intracellular molecular switches which further affect actin modifying proteins. Those molecular switches are RhoGTPases that belong to the Ras super family and are only active in the GTP bound state [38]. The transition between GDP and GTP binding, and thus its activity, is modified by guanine nucleotide exchange factors (GEFs) towards GTP binding state and GTPase activating proteins (GAPs) favoring the GDP bound state. The most important RhoGTPases in migration are Rac1, Cdc42 and RhoA (Figure 1.6). Rac1 is the main factor for the formation of lamellipodia. Rac1 activates the branching factor Arp2/3 via WAVE as well as via Cortactin which recruites the Arp2/3 complex leading to a thick branched filament network. For the formation of filopodia, the RhoGTPase Cdc42 is responsible which activates the LIM kinase (LIMK) via PAKs, finally, inhibiting the actin severing protein Cofilin. Stress fibers are regulated by the RhoGTPase Rho which mediates contraction by the inhibition of Cofilin via the Rho associated protein kinase (ROCK) and LIMK as well as the activation of myosin via ROCK and myosin light chain phosphatase (MLC phosph.) and the nucleator mDia. [39, 40, 41]

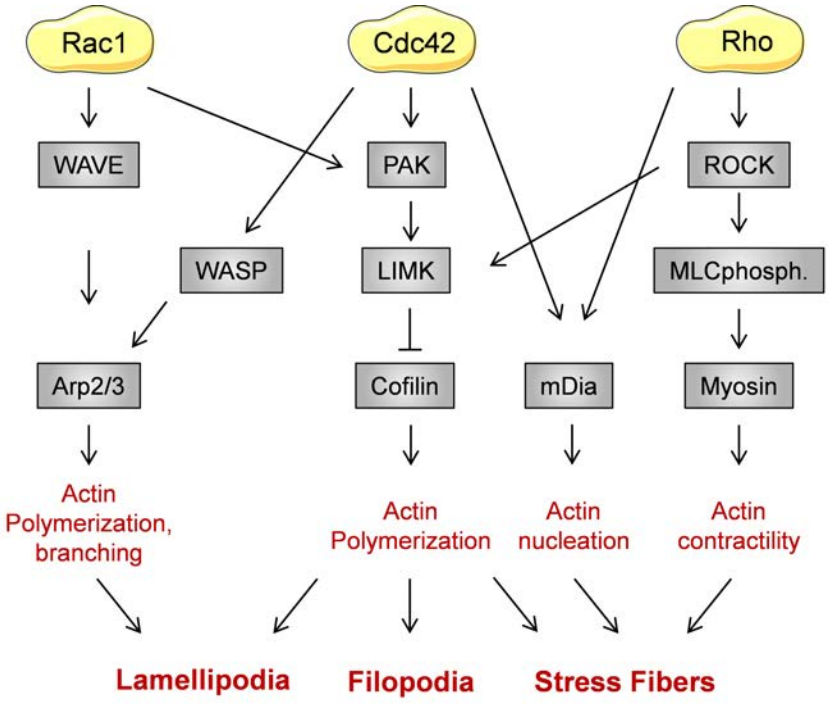

Figure 1.6: **Signaling downstream to RhoGTPases Rac1, Cdc42 and Rho.**

The RhoGTPases itself are activated via extracellular stimuli that are transmitted either by tyrosin kinases, G protein-coupled receptors or integrins. Thus, extracellular growth factors bind to the membranous receptor tyrosine kinase (RTK), which autophosphorylates and activates PI3 kinases (PI3K). PI3K converts phosphatidylinositol-4,5-bisphosphate (PIP2) to phosphatidylinositol-3,4,5-triphosphate (PIP3) which binds GEFs, activates them, finally leading to RhoGTPase activation. Other stimuli like lysophosphatidic acid (LPA) bind to G protein-coupled receptors, thereby, releasing G12/13 which in turn binds and activates Rho-GEFs. [42, 43]

Additionally to soluble factors, extracellular matrix can also lead to RhoGTPase activation like during adhesion (Figure 1.7 A). The binding of integrins to ECM activates integrins allowing the attachment of signaling molecules in the cytoplasm. Thus, after new attachment, the focal adhesion kinase binds the intracellular part of integrins leading to autophosphorylation of FAK. Consequently, Src is recruited resulting in further phosphorylations of FAK, establishing additional protein binding sites and full activity of the FAK/Src complex [44]. This complex further phosphorylates other proteins like p130Cas or paxillin which then bind GEFs to an active complex or phosphorylates GEFs to activate Rac1 for cell spreading. At later stages of adhesion, integrin-mediated activation of GEFs induces RhoA activation initiating contractility [45, 46]. In addition to adhesion, mechanical stimuli, stretching or shear stress, activate Rho via integrins at which Vav2 is one of the involved GEFs (Figure 1.7 B) [47, 48].

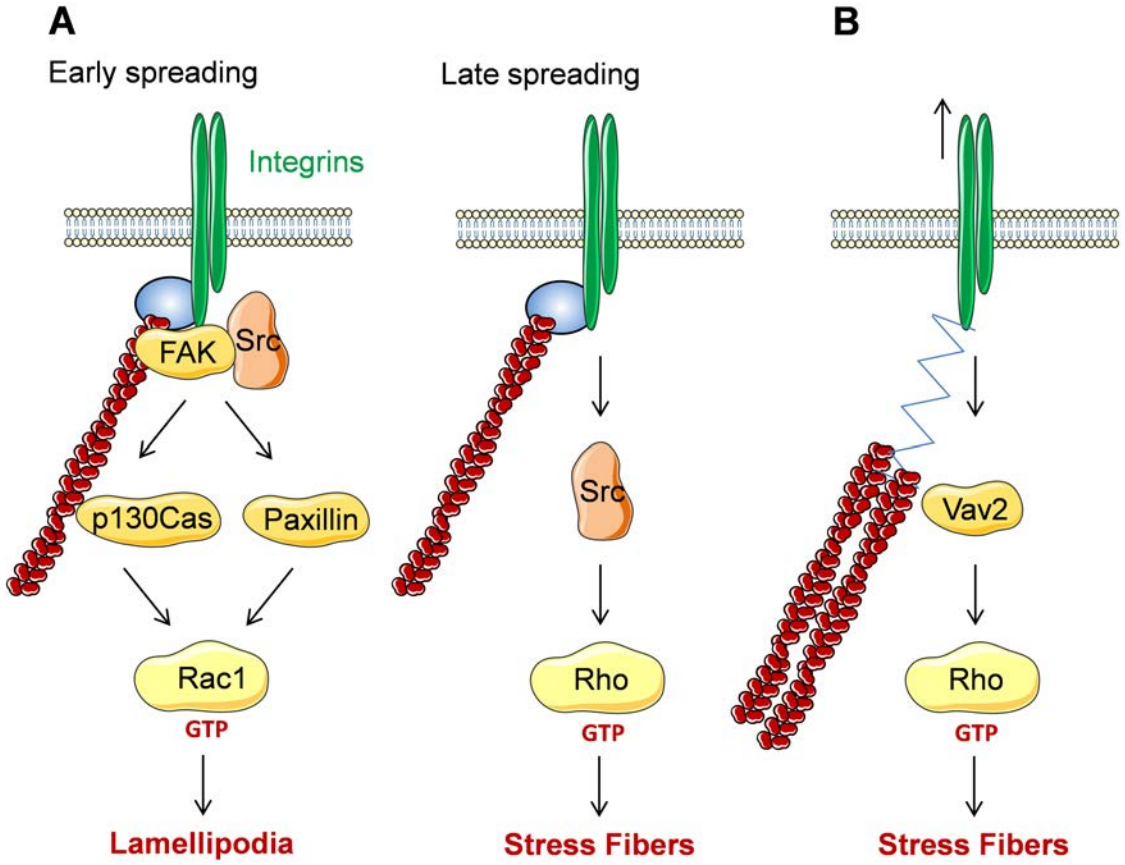

Figure 1.7: **Activation of RhoGTPases via integrin signaling.** A: Activation of RhoGTPases during cell spreading. In the early phase of spreading, the complex of FAK and Src forms at the intracellular domain of integrins and phosphorylates p130Cas and Paxillin which, finally, activate GEFs and, thus, Rac1. At later stages, Src initiates Rho activity. B: Activation of Rho via force. Either extracellular or intracellular forces can induce Rho activity via the GEF Vav2.

1.7 Aim of the study

Tumor angiogenesis and cancer cell metastasis are major processes contributing to the progression of cancer. Both processes involve the migration of cells and, thus, high plasticity of the actin cytoskeleton. Therefore, actin is an interesting target to adress for the inhibition of angiogenesis or metastasis. Chondramide is a natural compound from myxobacteria that binds actin and disturbs actin turnover.

The aim of this study was to evaluate the potential of Chondramide to inhibit angiogenesis and metastasis. For this purpose, endothelial cells should be tested on characteristic angiogenic features like proliferation, migration and tube formation under Chondramide treatment. Next, the responsible actin structures should be evaluated on their response on Chondramide treatment to explain functional changes. Further, the signaling cascades involved in the migration process and actin regulation were tested on their response to Chondramide treatment.

Concerning metastasis, the impact of Chondramide on cancer cell migration and invasion was tested. To answer the question, how functional changes are generated by Chondramide, responsible actin structures were investigated as well as important signaling components. Further, the consequences of Chondramide on the migration of cancer cells in a 3D environment were evaluated.

Concluding, this work aimed to investigate the anti-angiogenic and anti-metastatic potential of the actin binding compound Chondramide and to examine the underlying intracellular mechanisms causing the cellular response.

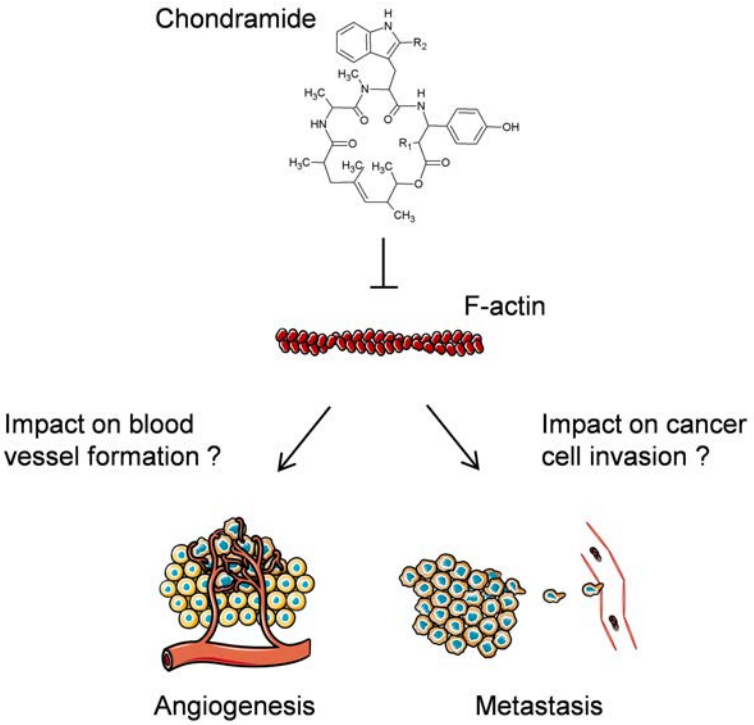

Figure 1.8: **Aim of the study.** The myxobacterial compound Chondramide binds actin and leads to its overpolymerization. The impact of Chondramide on tumor angiogenesis and metastasis was evaluated. Thereby, Chondramide was tested on its impact on cellular functionality, the corresponding actin structures and the underlying signaling.

2: Material and Methods

2.1 Materials

2.1.1 Compounds

Chondramides were isolated and provided from the group of Rolf Müller [49]. Chondramide A and B (ChA, ChB) were dissolved and stored in DMSO and dissolved in growth medium for experiments containing DMSO at a maximum of 0.1% (v/v). Jasplakinolide (Jk) was purchased from Enzo Life Sciences (Lörrach, Germany) and Cytochalasin D (CytoD) from AppliChem (Darmstadt, Germany).

2.1.2 Reagents, dyes and inhibitors

Table 2.1: **Reagents and dyes**

Reagent	**Producer**
Accustain paraformaldehyde	Sigma Aldrich, Taufkirchen, Germany
Bovine serum albumin (BSA)	Sigma Aldrich, Taufkirchen, Germany
Bradford Reagent™	Bio-Rad, Munich, Germany
Dimethylsulfoxide (DMSO)	AppliChem, Darmstadt, Germany
Epidermal growth factor (EGF)	PeproTech Inc., Rocky Hill, NJ, USA
EGTA-K	AppliChem, Darmstadt, Germany
FluorSave™ Reagent mounting medium	Merck, Darmstadt, Germany
Formaldehyde, 16% ultrapure	Polysciences Europe GmbH, Eppelheim, Germany
Glutaraldehyde	Merck, Darmstadt, Germany
Matrigel™	BD Biosciences, Heidelberg, Germany
Non-fat dry milk powder (Blotto)	Carl Roth, Karlsruhe, Germany
Page Ruler™Prestained Protein Ladder	Fermentas, St. Leon-Rot, Germany
Propidium iodide	Sigma Aldrich, Taufkirchen, Germany
Triton X-100	Merck, Darmstadt, Germany
Tween® 20	BDH/Prolabo®, Ismaning, Germany

All other biochemicals and dyes used in this work were purchased from Sigma-Aldrich, AppliChem, Carl Roth or Merck.

Table 2.2: **Inhibitors used in the study**

Inhibitor	**Producer**
Aprotinin	Sigma Aldrich, Taufkirchen, Germany
Complete® mini EDTA free	Roche diagnostics, Penzberg, Germany
Leupeptin hemisulfate salt	Sigma-Aldrich, Taufkirchen, Germany
Na_3VO_4	ICN Biomedicals, Aurora, OH, USA
NaF	Merck, Darmstadt, Germany
Phenylmethylsulfonyl fluoride (PMSF)	Sigma Aldrich, Taufkirchen, Germany
Saracatinib (AZD-0530)	Selleck Chemicals, Houston, USA

Table 2.3: **Cell culture reagents**

Cell culture reagent	**Producer**
Amphotericin B 250 μg/ml	AppliChem, Darmstadt, Germany
Collagen G	Biochrom AG, Berlin, Germany
Collagenase A	Roche, Mannheim, Germany
Dulbecco's modified Eagle's medium (DMEM)	Sigma Aldrich, Taufkirchen, Germany
Endothelial Cell Growth Medium (ECGM) with Supplement Mix C-39215	PromoCell, Heidelberg, Germany
FCS gold	PAA Laboratories, Pasching, Austria
FCS	PAN Biotech, Aidenbach, Germany
M199 medium	PAA Laboratories, Pasching, Austria
Penicillin/Streptomycin 100x	PAA Laboratories, Pasching, Austria
RPMI 1640	PAN Biotech, Aidenbach, Germany
Trypsin	PAN Biotech, Aidenbach, Germany
EDTA disodium salt dihydrate	Carl Roth, Karlsruhe, Germany

2.2 Cell culture

2.2.1 Solutions and reagents

For the cultivation of cells, solutions were used in the following compositions:

Table 2.4: **Cell culture solutions**

Solution	**Composition**
PBS (pH 7.4)	NaCl (123.3 mM), Na_2HPO_4 (10.4 mM), KH_2PO_4 (3.2 mM) in H_2O
PBS+ Ca^{2+}/Mg^{2+} (pH 7.4)	NaCl (136.9 mM), KCl (2.7 mM), Na_2HPO_4 (8.1 mM), KH_2PO_4 (1.5 mM), $MgCl_2$ (0.5 mM), $CaCl_2$ (0.7 mM) in H_2O
ECGM	Supplement Mix (4.7%), FCS gold (10%), Amphothericin B (0.25%), Penicillin (10,000 U/ml) Streptomycin (10%) in ECGM
DMEM	FCS gold (10%), Penicillin (10,000 U/ml), Streptomycin (10%) in DMEM
RPMI	FCS gold (10%), non-essential amino acid (1%), pyruvate (1%), human insulin (10 μg/ml) in RPMI 1640
Stopping medium	FCS (10% in M199
Trypsin/EDTA	Trypsin (0.05%), EDTA (0.02%) in PBS
Collagen G	Collagen G (0.001%) in PBS
Collagenase A (HUVEC isolation)	Collagenase A (0.01%) in PBS+ Ca^{2+}/Mg^{2+}

2.2.2 Endothelial cells

As endothelial cell line CDC/EU.HMEC-1 (HMEC-1) were used. The cell line was established from primary isolated human dermal microvascular endothelial cells (HMEC) immortalized via transfection of BR-322-based plasmid containing the coding region for the simian virus 40 A gene product [50, 51]. HMEC-1 were kindly provided by Centers for Disease Control and Prevention (Atlanta, GA, USA), passaged twice a week in a ratio of 1:4 and used until passage 12.

For adhesion related experiments, the primary cells, human umbilical vein endothelial cells (HUVECs), were used isolated from the umbilical cord vein. Human umbilical cords were kindly provided by Klinikum München Pasing, Wolfart Klinik Gräfelfing, Frauenklinik Dr. Krüsmann München and Rotkreuzklinikum München in accordance with the declaration of Helsinki. Umbilical cords were stored in PBS+ Ca^{2+}/Mg^{2+} containing Penicillin (100 U/ml) and Streptomycin (100 μg/ml) at 4°C for maximal 1 week until usage. For isolation, the umbilical vein was first washed with PBS+ Ca^{2+}/Mg^{2+}, filled with 0.1 g/l collagenase A, and incubated for 45 min at 37°C. Collagenase was stopped and endothelial cells were washed out by flushing the vein with stopping medium. For cultivation, endothelial cells were centrifuged (1000 rpm, 5 min, RT), resolved in ECGM and plated in a 25 cm^2 flask. After reaching confluency, cells were transfered to a 75 cm^2 flask. For experiments, HUVECs were used at passage 3.
All endothelial cells (ECs) were cultured under constant humidity at 37°C and with 5% CO_2 in an incubator (Heraeus, Hanau, Germany). As cell culture medium, endothelial cell growth medium (ECGM, Promocell, Heidelberg, Germany) was used.

2.2.3 Cancer cells

Concerning metastasis, the highly invasive cancer cell line MDA-MB-231 was used. This cell line, isolated from breast carcinoma metastasis via pleural efusion, shows negative expression of estrogen, progesterone and HER-2 receptor and a highly invasive mesenchymal phenotype [52, 53, 54]. MDA-MB-231 cells were purchased from Cell Line Services (Eppelheim, Germany), cultivated in DMEM and passaged twice a week in a ratio of 1:10.

For comparison of migration inhibition, the cancer cell lines MCF-7 (breast cancer), L3.6pl (pancreatic cancer) and HUH-7 (hepatic cancer) were used. HUH-7 cells (JCRB0403, JCRB, Tokyo, Japan) were cultured in DMEM and passaged twice a week in a ratio of 1:5. MCF-7 (ACC 115, DSMZ, Braunschweig, Germany) were cultured in RPMI and passaged twice a week in a ratio of 1:10. L3.6pl were provided by Christine J. Bruns (Department of Surgery, Klinikum Grosshadern, LMU Munich, Germany), cultivated in RPMI and passaged twice a week in a ratio of 1:10.

All cancer cell lines were cultured under constant humidity at 37°C and with 5% CO_2 in an incubator (Heraeus, Hanau, Germany).

2.2.4 Passaging

For passaging, medium was removed, cells were washed twice with PBS, trypsin/ethylene diamine tetraacetic acid (EDTA) (T/E) was added and incubated at 37°C. After 3 min incubation, digestion was stopped by adding stopping medium. Cells were centrifuged (1000 rpm, 5 min, RT), resuspended in ECGM and, finally, transfered to a new flask or seeded for experiments.

2.2.5 Freezing and thawing

For long time storage, confluent HMEC-1 or cancer cells from a 75 cm^2 flask were trypsinized, centrifuged (1000 rpm, 5 min, RT) and resuspended in 3 ml ice-cold freezing medium. 1.5 ml aliquots were frozen in cryovials and stored at -80°C for 24 h before being moved to liquid nitrogen for longtime storage.
In order to thaw cells, cryovials were warmed up to 37°C and the content was immediately dissolved in the appropriate, prewarmed culture medium. DMSO was removed via centrifugation, cells were resuspended in cell culture medium and transferred to a 75 cm^2 flask.

2.3 Angiogenesis assays

2.3.1 Proliferation assay

HMEC-1 (1.5 x 10^3 cells/well) were seeded in a 96-well plate. After 24 h, cells were treated with the indicated concentrations of Ch and incubated for 72 h. Finally, cells were washed with PBS, incubated with 100 μl/well crystal violet solution (0.5% (w/v) crystal violet, 20% (v/v) methanol in H_2O) for 10 min, washed and dried. For solvation of crystal violet, 100 μl/well ethanol/Na-citrate solution (50% ethanol, 50% 0.1 M Na-Citrat in H_2O) were added, incubated for 5 min and measured at 540 nm using a microplate reader (Sunrise, Tecan, Männedorf, Switzerland).

2.3.2 Scratch assay

For scratch assay, confluent HMEC-1 were scratched using a pipette tip and treated as indicated. Endothelial cells were allowed to migrate for 13 h, then fixed with 4% (v/v) paraformaldehyde (p-FA) and images were taken using TILLvisION system (Lochham, Germany) in connection with an Axiovert 200 microscope (Zeiss, Jena, Germany). Images were analyzed by Wimasis GmbH (Munich, Germany). Migration was quantified as the percentage of the cell covered area compared to the total image area.

2.3.3 Chemotaxis assay

For chemotaxis assay, 50 x 10^3 HMEC-1 were seeded in a μ-slide chemotaxis (ibidi GmbH, Munich, Germany). After 2 h, a gradient between 0 to 30% (v/v) FCS was applied according to manufacturer's instructions. Images were taken every 10 min for 20 h using an open U-iMIC microscope (TILL Photonics, GmbH, Gräfelfing, Germany), 10x objective. Images were analyzed employing the ImageJ plugin Chemotaxis tool.

2.3.4 Tube formation assay

In order to analyze the ability of endothelial cells to form tube structures, tube formation assay was performed. Therefore, 11 x 10^3 HMEC-1 were seeded on matrigel (MatrigelTM, Schubert&Weiss-OMNILAB, Munich, Germany) in an angiogenesis slide from ibidi (Munich, Germany), treated as indicated and incubated for 15 h. Images were taken using the TILLvisION system. Analysis of images was performed by Wimasis GmbH (Munich, Germany). For time lapse imaging, the open U-iMIC microscope was used with a stage incubator. As parameters of tube formation, tube length, number of nodes and number of tubes were analyzed.

2.3.5 Adhesion assay

Pretreated HUVECs were trypsinized, suspended in DMSO or Ch containing ECGM and allowed to adhere on fibronectin or collagen for 30 min. Cells were fixed with 4% (v/v) p-FA and stained for F-actin. Images were taken (10x objective; Zeiss LSM 510 META

confocal microscope, Jena, Germany) and counted for adhering cells. Cell morphology was distinguished in normal spreading cells (normal), irregular shaped cells, showing non-symmetrical spreading (irregular), and completely rounded cells (globular).

2.4 Metastasis assays

2.4.1 Scratch assay

The migration of cancer cells was analyzed analogue to endothelial cell migration in scratch assay. Only the time for scratch recovery was different for each cell line at which MDA-MB-231 cells were incubated for 24 h, MCF-7 for 30 h and L3.6pl as well as HUH-7 cells for 27 h.

2.4.2 Boyden chamber assay

In order to follow cancer cell migration towards a growth factor gradient, Boyden chamber assay was used. For this purpose, 5 x 10^4 MDA-MB-231 cells were seeded per well in a Boyden chamber (Corning, New York, USA) without FCS. For negative control, the lower compartment was filled with medium lacking FCS, whereas for positive control and treated samples, the lower compartment was filled with full medium containing 10% (v/v) FCS. After 16 h, cells were fixed and stained with crystal violet/methanol (see proliferation assay). Cells on top of the filter were removed with a q-tip and bottom sides were photographed using an Axiovert25 microscope (Zeiss), 10x objective, and a Canon EOS 450C camera (Tokyo, Japan). Images were analyzed using the ImageJ plugin cell counter.

2.4.3 Invasion assay

The invasion assay was performed analogue to Boyden chamber assay except for filters being filled with 100 μl 10% (v/v) matrigel (Schubert&Weiss-OMNILAB, Munich, Germany). Matrigel was allowed to polymerize for 1 h at 37°C before cell seeding. Cellular invasion was incubated for 48 h.

2.4.4 Adhesion assay

Pretreated MDA-MB-231 cells were trypsinized, suspended in DMSO or Ch containing medium and allowed to adhere on fibronectin, collagen G or plastic for 1 h. Cells were fixed with 4% (v/v) p-FA and stained for F-actin. Images were taken on a Zeiss LSM 510 META confocal microscope (10x objective) and counted for adhering cells.

2.5 Flow cytometry (FACS)

Flow cytometry was used to measure the amount of apoptotic cells or surface proteins.

2.5.1 Measurement of sub-diploid DNA content

To detect apoptotic cells, sub-diploid DNA content (i.e. fragmented nuclei) was measured as described by Nicoletti et al. [55]. Thereby, HMEC-1 were seeded in a 24-well plate (70 x 10^3 cells/well), grown over night and treated with Ch. After 48 h, cells were harvested (200 μl T/E per well for 2 min, 500 μl stopping medium), transfered to a FACS tube and washed with cold PBS (1ml/tube, centrifugation: 600g, 10 min, 4°C). For nuclei staining, 250 μl per well HFS-PI solution (0.1% (v/v) Triton X-100, 0.1% (w/v) sodium citrate, 50 μg/ml propidium iodide) was added and incubated for 45 to 60 min. Sub-diploid DNA content was measured by flow cytometry using a FACSCalibur (Becton Dickinson, Heidelberg, Germany) and analyzed using the Flow cytometry analysis software FlowJo 7.6.

2.5.2 Measurement of membraneous, extracellular proteins

For the measurement of extracellular integrins, HUVECs were seeded in a 24-well plate (60 x 10^3 cells/well), grown over night and stimulated with Ch for 4 h. Cells were harvested on ice (see 2.5.1), transfered to a FACS tube and washed (2.5.1). For staining, 30 μl/tube of antibody for total integrin β1 (1:400 in 0.01% BSA/PBS, Santa Cruz Biotechnology Inc., Santa Cruz, CA, USA) or active integrin β1 (1:400 in 0.01% BSA/PBS, Abcam Inc., Cambridge, MA, USA) were added per sample and incubated for 45 min at 4°C. Samples were washed and incubated with secondary antibody (Alexa Fluor® 488 Goat anti-mouse IgG, Molecular Probes, Darmstadt, Germany, 1:400 in 0.01% BSA/PBS) for 45 min protected from light.

After a final washing step, samples were resuspended in 250 μl PBS and analyzed by flow cytometry using a FACSCanto II (Becton Dickinson, Heidelberg, Germany) and the mean fluorescence was calculated using the Diva-Software of BD Bioscience (San Jose, CA, USA).

2.6 Propidium iodide staining for microscopy

In order to test the membrane integrity, propidium iodide staining of adherent cells was performed. Therefore, 30 x 10^3 HMEC-1 were seeded in a 24-well plate and incubated over night. After Ch stimulation, propidium iodide was added to the medium to a final concentration of 10 μg/ml for 15 min. For positive control, additional Triton X-100 was added (final concentration 0.02% (v/v) in PBS). Pictures were taken on a fluorescent microscope with 10x objective.

2.7 Transfection of cells

For the transfection of endothelial cells the Targeffect-HUVEC kit (Targetingsystems, El Cajon, CA, USA) was used. 70 x 10^3 HUVECs were seeded in a μSlide from ibidi and incubated over night. For transfection complex, 800 μl DMEM were supplemented with 800 ng plasmid DNA (pLifeAct-TagGFP, ibidi), 1.6 μl F2 reagent and 3.2 μl virofect enhancer at which flicking the tube 10x after each addition. After transfection complex formation, the mixture was incubated 25 min at 37°C, medium of cells was removed and 200 μl of transfection solution was added and incubated for 2 to 3 h at 37°C.

2.8 Microscopy

2.8.1 Microscopy with fixed cells

In order to visualize the localization of a certain protein within the cell, immunohistochemistry was performed.

Cells were seeded and treated in μ-slides from ibidi. For staining, samples were washed once with PBS+ (RT), fixed (see below) and washed again with standard PBS. Permeabilization followed if necessary with 0.1% (v/v) Triton X-100 for 2 min at RT and a washing step of 10 min with PBS. Next, samples were blocked with 0.2% (v/v) BSA (PBS) for 15 min at RT before incubation with primary antibody. Primary antibodies (150 μl/well) were added in dilutions as indicated in 0.2% (v/v) BSA (Table 2.5) and incubated either for 1 h at RT or over night at 4°C, shaking. After washing three times with PBS for 5 min each, the secondary antibody was applied (150 μl/well, 0.2% (v/v) BSA) together with rhodamin-phalloidin and Hoechst for 45 min at RT, shaking. Samples were washed thrice, 5 min each, with PBS, and, finally, sealed with mounting medium (FluorSave^{TM} Reagent, Merck Millipore) and cover slip. Samples were kept at 4°C for longer storage.

For fixation, different methods were used depending on the target recognition of the applied antibody. For fixation with p-FA, samples were incubated either with 4% (v/v) p-FA for 10 min at RT or with 1% (v/v) p-FA for over night at 4°C and permeabilized with Triton X-100 afterwards. In case of aceton or methanol fixations, samples were incubated with prechilled aceton or methanol at -20°C for 10-15 min without incubation with Triton afterwards.

In case of single F-actin staining, samples were treated as described, however, blocking and primary antibody were skipped and rhodamin-phalloidin was solved in PBS.

Images were obtained using a Zeiss LSM 510 META confocal microscope (Zeiss, Jena, Germany) or a Leica TCS SP8 (Leica Microsystems, Wetzlar, Germany).

Table 2.5: **Primary antibodies for immunohistochemistry**

Antibody	Provider	Fixation	Dilution
Anti-Cortactin (3503)	Cell signalling	p-FA	1:100
Anti-Integrin $\alpha 2\beta 1$ (ab30483)	Abcam	p-FA	1:1000
Anti-Integrin $\alpha 5$ (AB1928)	Millipore, Upstate	p-FA	1:1000
Anti-LAMP-1 (H4A3)	Dev. St. Hybridoma	p-FA	1:400
Anti-pp(T18S19)-MLC (3674)	Cell signalling	p-FA	1:200
Anti-p21-Arc (612234)	BD Biosciences	Methanol	1:100
Anti-Rab5A (S-19, sc-309)	Santa Cruz	p-FA	1:200
Anti-α-tubulin (ab18251)	Abcam	Aceton	1:400
Anti-γ-tubulin (T 6557)	Sigma	Methanol	1:2000
Anti-VE-cadherin (sc-9989)	Santa Cruz	p-FA	1:400

Table 2.6: **Secondary antibodies or dyes for immunohistochemistry**

Antibody/Dye	Provider	Dilution
Alexa Fluor 488 chicken anti-goat IgG (H+L)	Invitrogen	1:400
Alexa Fluor 488 goat anti-mouse IgG (H+L)	Invitrogen	1:400
Alexa Fluor 488 goat anti-rabbit IgG (H+L)	Invitrogen	1:400
Hoechst (bisBenzimide H33342)	SigmaAldrich	1.400
Rhodamin-phalloidin (R 415)	Invitrogen	1:400

2.8.2 Life cell imaging

To follow actin dynamics during the migration process, life cell imaging was performed. HUVECs were transfected with pCMV-LifeAct-TagGFP (ibidi, Munich, Germany) and seeded in μslides. Upon confluency, the cell monolayer was scratched and samples were mounted on an open U-iMIC microscope with climate chamber. Images were taken every 10 min for several hours. Movies were analyzed using ImageJ.

2.8.3 Histological stainings

For the visualization of tumoral vasculature, cryosections were stained. Tumors embedded in FrozenSection Medium Neg50 (Thermo Scientific) were sliced into sections of 10 μm. Cryo-slices were allowed to dry for 15 min at RT, washed with PBS for 2 min and fixed with 4% (v/v) p-FA for 10 min at RT. Permeabilization and blocking occured in one step with 2% (v/v) BSA, 0.5% (v/v) Triton X-100 in PBS for 30 min at RT. CD31 was stained with a rat anti-mouse CD31 antibody (553370, BD Biosciences, San Jose, USA, 1:100) over night at 4°C. Slices were washed twice for 7 min with PBS and secondary antibody (goat anti-rat 546,

1:400) was mounted for 2 h at RT together with Hoechst (1:400). Samples were washed (2x, 7 min, PBS), washed once with water and sealed with mounting medium and cover slip. Images were taken using a Zeiss LSM 510 META confocal microscope.

2.9 Measurement of cellular contractility

For the measurement of cellular contractility, an assay was performed adapted from Poincloux et al. [56]. Thereby, cells were embedded in matrigel containing fluorescent beads. Cellular force on the surrounding matrix results in bead movement which can be tracked by time lapse imaging and analyzed afterwards.

2.9.1 Contractility assay

To this end, MDA-MB-231 cells were pretreated with Ch and labeled with CellTracker^{TM} Red (LifeTechnologies, Carlsbad, CA, USA) (5μM) for 30 min. Next, yellow-green microbeads of 1 μm diameter, 2% solids (LifeTechnologies) were mixed with matrigel in a ratio of 1:4 (v/v) on ice. The bead/matrigel mixture was mixed with pretreated, labeled MDA-MB-231 cells, 5 x 10^6 cells/ml, in a ratio of 2:1 (v/v) and pipetted in an angiogenesis slide (ibidi). Matrigel containing cells was allowed to polymerize for 1 h at 37°C, 5% CO_2 in humidified atmosphere, before samples were covered with culture medium. Images were taken using an open U-iMIC fluorescent microscope (TILL Photonics GmbH, Gräfelfing, Germany) with a climate chamber and 20x objective. One z-stack per well was recorded and chosen cells had a minimum distance of 20 μm to the edge of matrigel and sufficient space between cells to not disturb bead movement. Stacks of 5 slices around the cell equatorial plane with a 2 μm distance were taken over 4 h with 15 min intervals.

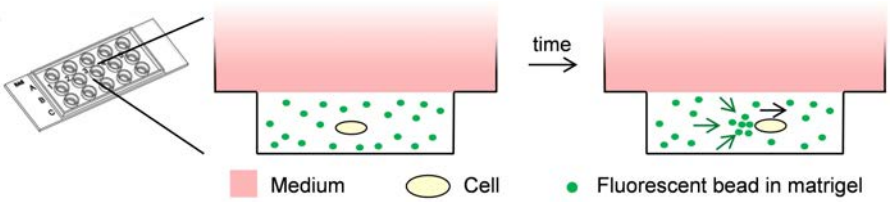

Figure 2.1: **Scheme of experimental setting for contractility assay.**

2.9.2 Image processing

Recorded stacks were processed for further analysis via imageJ. First, three out of five optical slices around the equatorial plane of the cell were selected (command: make substack) and projected in one plane (command: maximum intensity projection), once for cell channel and once for bead channel. Shifts in the xy plane were removed (plug in: image stabilizer) first for the beads, and the recorded shift was tranfered to the cell stack. Next, the two stacks, beads and cells, were fused to an hyperstack and croped to standardized 300 x 300 px with one cell at the image center. The bead channel was used for analysis.

2.9.3 PIV analysis

Movies of fluorescent beads were analyzed by particle image velocimetry (PIV) analysis performed by Matthias Zorn (Department of Physics, LMU, Munich).
Thereby, a customized MatPIV software package for Matlab was used. Interrogation windows were 32 x 32 pixels, i.e. 21 x 21 μm. A single iteration was performed with 62.5% overlap. The resulting velocity vectors were filtered with the set of filters included in the standard MatPIV package to smooth the vector fields. As the sample observation is restricted to 2D, z-components of the velocity are not seen and the PIV analysis only gives velocities projected into the observation plane. The obtained velocity field was averaged on each grid point over each frame of the observation period to further remove fluctuations that occur on short time scales. For quantitative comparison, the sum of values of particle displacement towards the cell center was calculated for each cell.
Minimum 13 cells per condition out of three independent experiments were recorded and analyzed.

2.10 Western blot analysis

For the detection of proteins in cell lysates, Western blot analysis was performed. Protein quantification of cell lysates was performed as described by Bradford [57]. Equal amounts of proteins were loaded on sodium dodecyl sulfate (SDS)-gels and separated via SDS-polyacrylamide gel electrophoresis (SDS-PAGE) using Bio-Rad System (Munich, Germany) (20 min: 100 V, 45 min: 200 V) [58]. For protein transfer from SDS gel to nitrocellulose membrane tank blot (Bio-Rad System) was used. For most proteins blotting occured at 1.5 h and 100 V except for MLC2 and its phosphorylated forms for which 1 h at 130 V was used. Protein detection was performed either using ECL detection system (Amersham Pharmacia Biotech) or Odyssey Infrared Imaging system version 2.1 (LI-COR Biosiences, Lincoln, NE, USA).

Table 2.7: **Western blot buffers**

Solution	**Composition**
RIPA lysis buffer	TrisHCl (pH 7.4) (50 mM), NaCl (150 mM) Nonidet NP 40 (1%), Deoxycholic acid (0.25 %) SDS (0.1%), Na_3VO_4 (0.3 mM) NaF (1 mM), β-glycerophsophate 3 mM Complete® mini EDTA free (4 mM)* PMSF (1 mM)*, H_2O_2 (0.5 mM)*, in H_2O
5x SDS sample buffer	TrisHCl (pH 6.8) (3.125 mM), Glycerol (10 ml) SDS (5%), DTT (2%) PyroninY (0.025%), in H_2O
3x Laemmli buffer	Tris/HCl (pH 6.8) (137.5 mM), Glycerol (30%) SDS (6%), Bromphenol blue (0.025%) β-Mercaptoethanol (12.5%)*
Electrophoresis buffer	Tris (4.9 mM), Glycine (38 mM) SDS (0.1%), in H_2O
Tank buffer 5x	TrisBase (240 mM), Glycine (195 mM), in H_2O
Tank buffer 1x	Tank buffer 5x (20%), Methanol (20%), in H_2O

*added right before usage

Table 2.8: **Primary antibodies for Western blot analysis**

Antigen	Source	Dilution	Solvent	Provider
Akt (9272)	rabbit	1:1000	5% Blotto	Cell Signalling
Akt pS473 (4051)	mouse	1:500	5% Blotto	Cell Signalling
EGF-R (4267)	mouse	1:500	1% Blotto	Cell Signalling
EGF-R pY1068 (3777)	rabbit	1:500	1% Blotto	Cell Signalling
Erk (9102)	rabbit	1:1000	5% Blotto	Cell Signalling
Erk pT202,Y204 (9106)	mouse	1:1000	5% Blotto	Cell Signalling
FAK (sc-1688)	mouse	1:500	5% Blotto	Santa Cruz
FAK pY397 (sc-11765-R)	rabbit	1:500	5% BSA	Santa Cruz
FAK pY576/577 (sc-21831-R)	rabbit	1:500	5% Blotto	SantaCruz
GAPDH (sc-69778)	mouse	1:1000	5% Blotto	Santa Cruz
MLC2 (FL-172) (sc-15370)	rabbit	1:500	5% Blotto	Santa Cruz
MLC2 p(S19) (3675)	mouse	1:1000	5% Blotto	Cell Signalling
Rac (23A8)	mouse	1:1000	5%Blotto, 0.1% Tw20	Merck Millipore
Rho (16116)	rabbit	1:667	3% BSA	Thermo Scientific
Src (2110)	mouse	1:1000	5% Blotto	Cell Singalling
Src pY416 (6943)	rabbit	1:1000	5% BSA	Cell Singalling
Vav2 (F-6) (sc-271442)	mouse	1:200	5% BSA	Santa Cruz
Vav2 pY172 (sc-16409-R)	rabbit	1:200	5% BSA	Santa Cruz

Table 2.9: **Secondary antibodies for Western blot analysis**

Antibody	Dilution	Solvent	Provider
Goat anti-mouse IgG1 HRP	1:1000	5% Blotto	Biozol
Goat anti-mouse HRP	1:10 000	5% Blotto	Dianova
Alexa Fluor® 680 Goat anti-mouse IgG	1:20 000	1% Blotto	Molecular Probes
Alexa Fluor® 680 Goat anti-rabbit IgG	1:20 000	1% Blotto	Molecular Probes

2.11 Pull down assay

For endothelial cells, one 75 cm^2-flask of confluent HUVECs was splitted into three 75 cm^2-flasks and grown for 16 h. The subconfluent cells were treated with Ch for 4 h and seeded freshly into 10 cm-dishes (coated with collagen G) and allowed to adhere for 30 min in order to activate RhoGTPases. All following steps were performed on ice at 4°C. Cells were lysed, harvested and a pull down assay according to manufacturer's protocol (Thermo Scientific, Bonn, Germany).

In case of cancer cells, MDA-MB-231 cells were seeded in a 6-well plate (400 x 10^3 cells/well) and grown for several hours. The activation of Rac1 and Rho was induced by adding 100 ng/ml EGF for 5 min to the medium followed by a pull down assay.

2.12 Statistical analysis

The number of independently performed experiments and the statistical tests used are stated in the respective figure legend. Graph data represent means $\pm$ SEM. Statistical analysis was performed with the software GraphPad Prism Version 5.04 (GraphPad Software, Inc., La Jolla, CA, USA). Statistical significance is assumed if $p \leq 0.05$.

3: Results

3.1 Chondramide diminishes angiogenesis *in vitro* and *in vivo*

3.1.1 Chondramide inhibits proliferation of endothelial cells at nanomolar concentrations

Initially, we examined the effect of Chondramide (Ch) on endothelial cell proliferation. Here, we could see that Ch inhibits the proliferation of HMEC-1 at nanomolar concentrations with an IC-50 value of 82 nM for ChA and 36 nM for ChB (Figure 3.1).

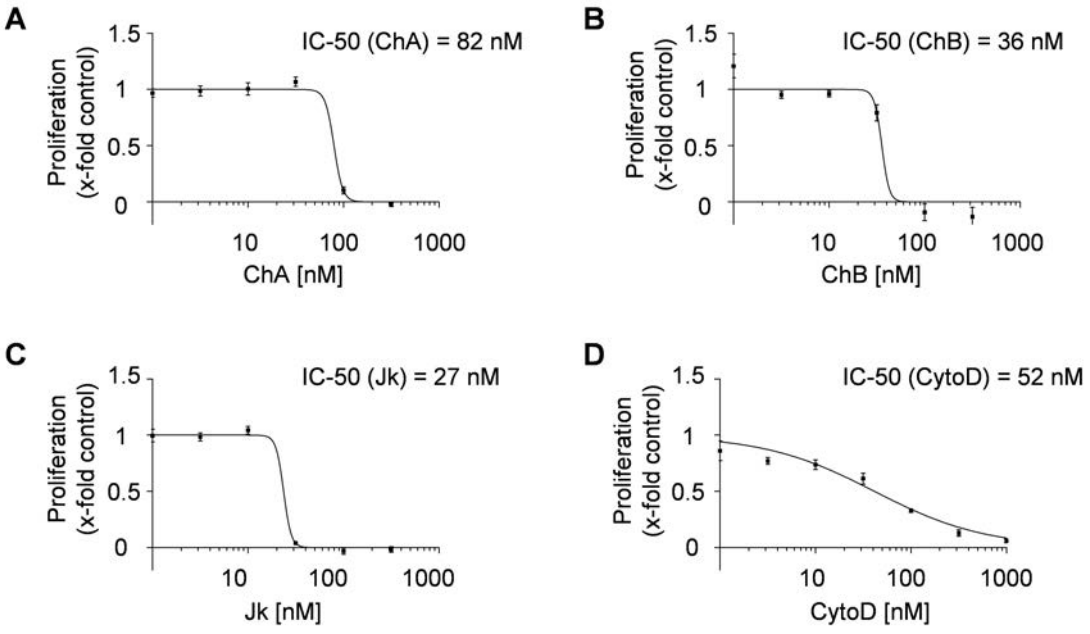

Figure 3.1: **Chondramide inhibits proliferation of endothelial cells at nanomolar concentrations.** Graphs of proliferation of endothelial cells are shown for ChA (A) and B (B) as well as the actin targeting substances Jasplakinolide (Jk, C) and Cytochalasin D (Cyto D, D). Half maximal inhibitory concentrations (IC-50) are inserted. (n=3)

Thus, both substances are very potent, however, ChB shows a slightly higher activity on proliferation. Interestingly, for both substances the curve showed an extreme sigmoidal curve slope meaning no effect up to 30 nM followed by an extreme drop to nearly zero at 100 nM revealing this as an interesting concentration range. Further, we compared the activity of Ch to the known actin-targeting substances Jasplakinolide (Jk) and Cytochalasin D (CytoD). As these showed an IC-50 of 27 nM (Jk) and 52 nM (CytoD), respectively, ChA and B are in a similar range of potency compared to established actin-targeting compounds.

3.1.2 Chondramide diminishes endothelial cell migration but not specifically chemotaxis

The migration of endothelial cells represents a major step in the process of angiogenesis. Therefore, we examined the effect of Ch on the migration of endothelial cells. First, a wound healing assay was performed. The migration of HMEC-1 towards the scratch was inhibited in a concentration dependent manner up to an inhibition to nearly 50% at 200 nM (Figure 3.2).

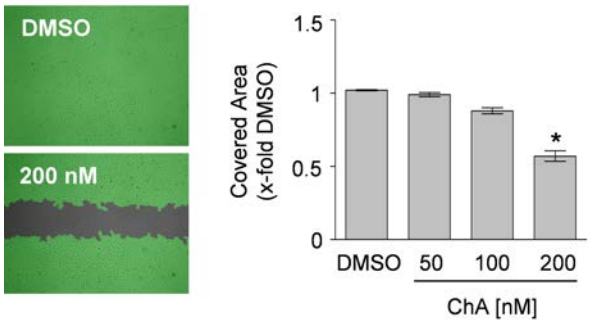

Figure 3.2: **Chondramide inhibits migration of HMEC-1 in a concentration dependent manner.** Left panel: Representative images are shown. The area covered with cells is displayed in green. Right panel: Analysis of images on cell covered area. (One-way ANOVA, Tukey post-test, * $p<0.05$, $n=3$).

Second, the impact on chemotactic properties in the migration towards a gradient of growth factors was tested. In the chemotaxis assay, migration was significantly inhibited at 100 nM as seen by a reduction of the mean velocity and the accumulated distance to less than 50% (Figure 3.3). The chemotactic ability was not affected specifically as the center of mass to-

wards the gradient was only reduced when cell migration was inhibited. Additionally, the total passed distance (accumulated distance) and the distance between start and end point (euclidian distance) were either not (30 nM) or both reduced (100 nM) indicating that Ch has an overall effect on cell motility but not the chemotactile properties specifically.

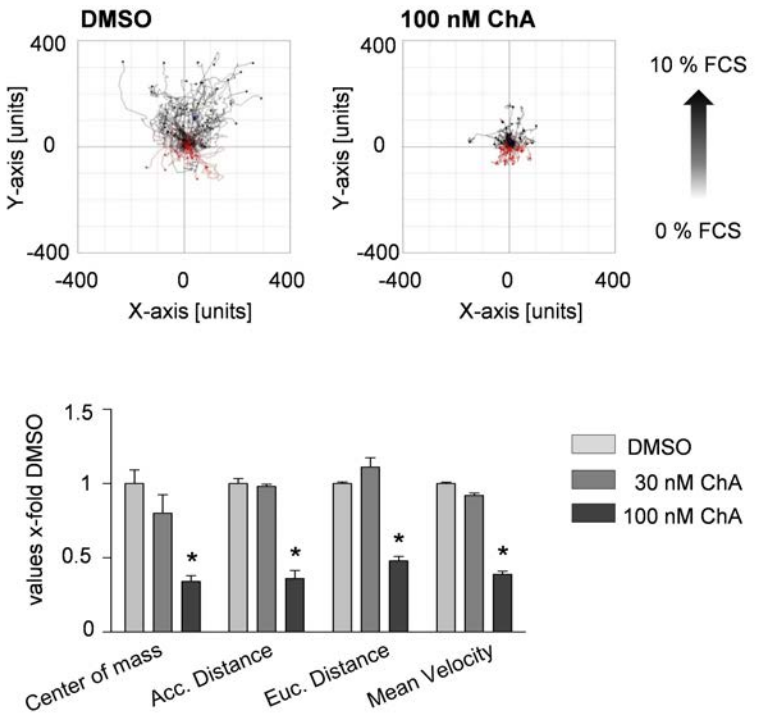

Figure 3.3: **Chondramide inhibits migration per se but does not diminish chemotactic properties of HMEC-1 specifically.** Upper panel: The analysis of one representative experiment is shown. Lower panel: Quantitative evaluation of the parameters center of mass, accumulated distance, euclidean distance and mean velocity. (One-way ANOVA, Tukey post-test, * $p<0.05$, n=4).

3.1.3 Chondramide disrupts tube formation in a concentration and time dependent manner

To simulate the process of angiogenesis *in vitro*, endothelial cells were seeded on matrigel to form tube like structures. End point images showed that the tube structure like in the DMSO control could not be established with rising concentrations of Ch (Figure 3.4).

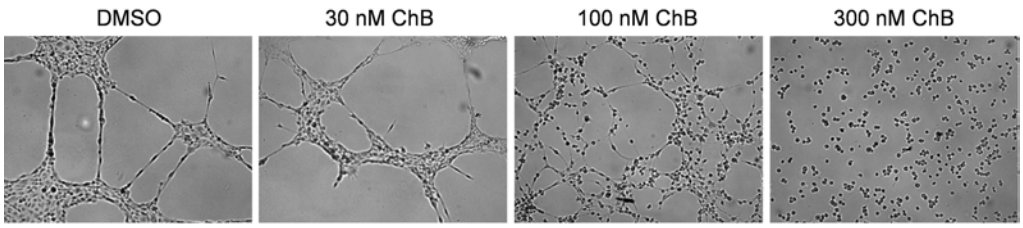

Figure 3.4: **Chondramide disturbs tube formation *in vitro* in a concentration dependent manner.** Representative images are shown (n=3, 10x objective).

To analyze the underlying process of Ch inhibiting the formation of tubes, we followed the process over time (Figure 3.5). Cells build a quite dense network of tubes after 4 h as seen by a high number of tubes, branching points and short tubes. Over time, this network maturates to a thinner network with fewer tubes, branching points and longer tubes as those fuse together. In the presence of 100 nM Ch, the establishment of the first network is still possible, however, the maturation later on is impaired as seen by less reduction of tubes and branching points. This effect was most obvious after 15 h. At 300 nM, cells could not even build the first network suggesting that the inhibitory effect of Ch is faster at higher concentrations and, thus, the process is concentration and time dependent (Figure 3.5).

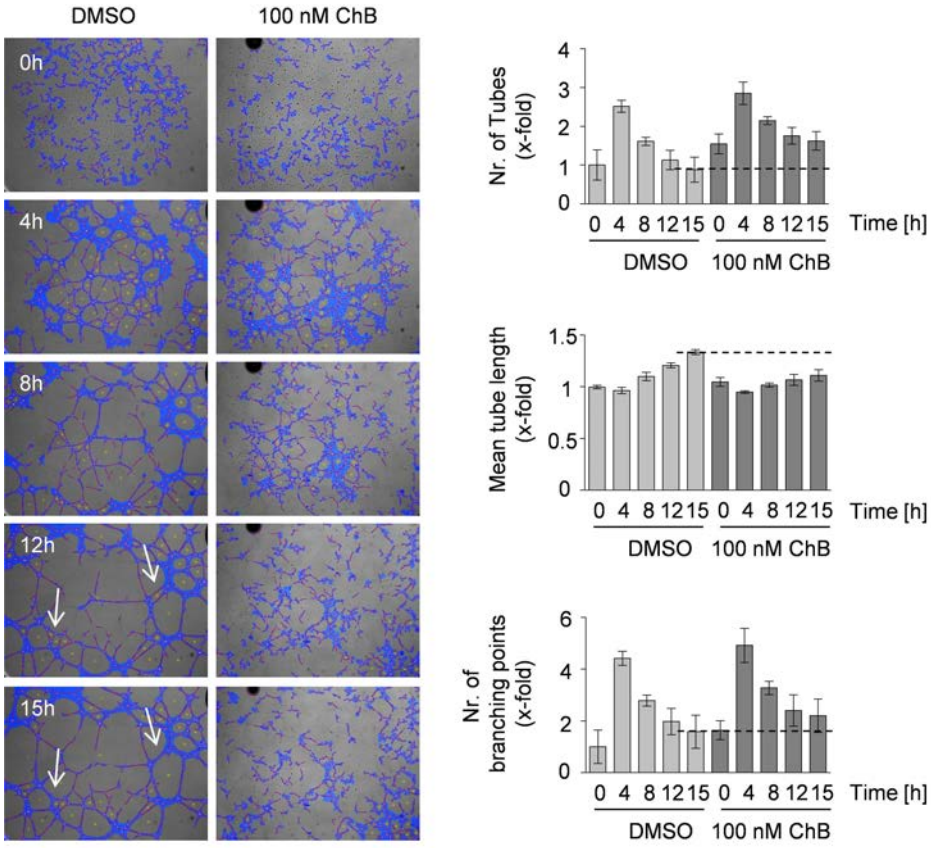

Figure 3.5: **The maturation of tubes is disturbed by Chondramide.** Number of tubes, number of branching points and tube length were analyzed over time. Left panel: Analyzed pictures at different time points (10x objective). Cell covered areas recognized by the software are indicated in blue, tubes in pink and branching points via yellow dots. Right panel: Graphs showing the development of analyzed parameters over time. Dashed line represents the respective values after treatment with DMSO for 15 h. (n=3)

Further, we wanted to know about the integrity of the formed tubes and stained cell-cell junctions via VE-Cadherin (Figure 3.6). Here, we could see that in tubes formed under Chondramide treatment (100 nM) the cell-cell contacts were clearly disrupted. This data indicates that Ch interferes with the maturation of tubes and development of cell-cell-contacts.

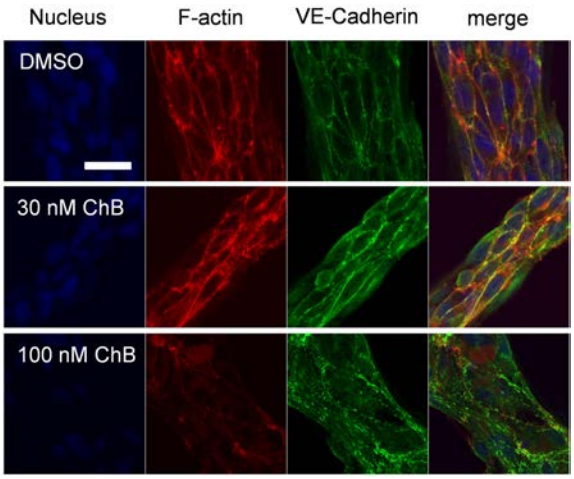

Figure 3.6: **Cell-cell contacts are disturbed in Chondramide treated tubes.** After tube formation assay (15 h), tubes were stained for F-actin (red), VE-Cadherin (green) and nuclei (blue). Yellow indicates an overlap of F-actin and VE-Cadherin. Representative images are shown. Bar represents 20 μm (n=3).

3.1.4 Chondramide leads to actin aggregation forming aggresomes

To get a first insight in the intracellular effect of Ch, stainings of the cytoskeleton were performed. The staining of the actin cytoskeleton revealed an aggregation of the fibrilous actin by Ch (Figure 3.7). At 30 nM Ch, aggregation was only seen close to the nucleus (arrow) and earliest after 4 h. However at 100 nM Ch, already after 2 h aggregation occurred in the cytoplasm followed by a complete retraction of the cells. In contrast, microtubules did not show any specific difference. At 30 nM and also at 100 nM microtubules changed only due to deformation of the whole cell.

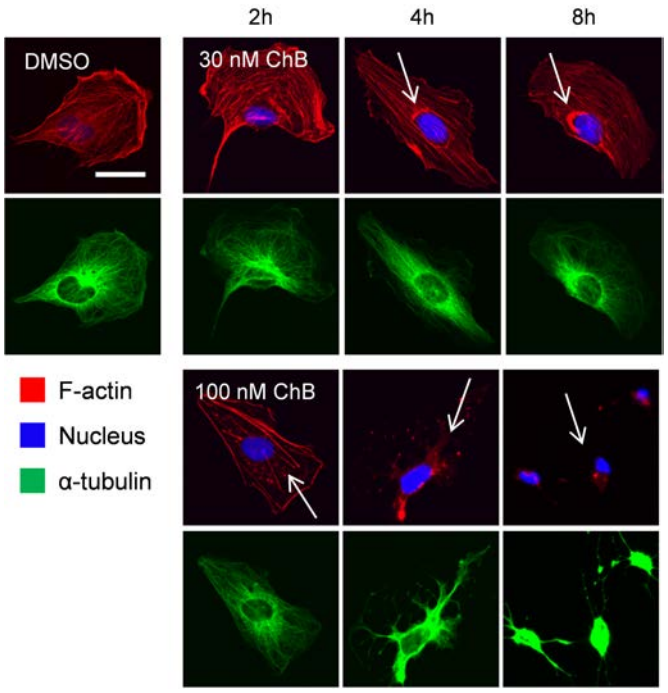

Figure 3.7: **Chondramide induces actin aggregation but does not disturb microtubules directly.** Proliferating HMEC-1 were treated with 30 or 100 nM ChB for the indicated time periods, fixed and stained for F-actin (upper panel) or α-tubulin (lower panel). Arrows indicate actin aggregates. Scale bar represents 20 μm (n=2).

These cells, retracted after Ch treatment, were still viable as propidium iodide staining was negative, cells recovered to normal cell size after substance removal and nicoletti assay showed less than 10% nuclear fragmentation (Figure 3.8).

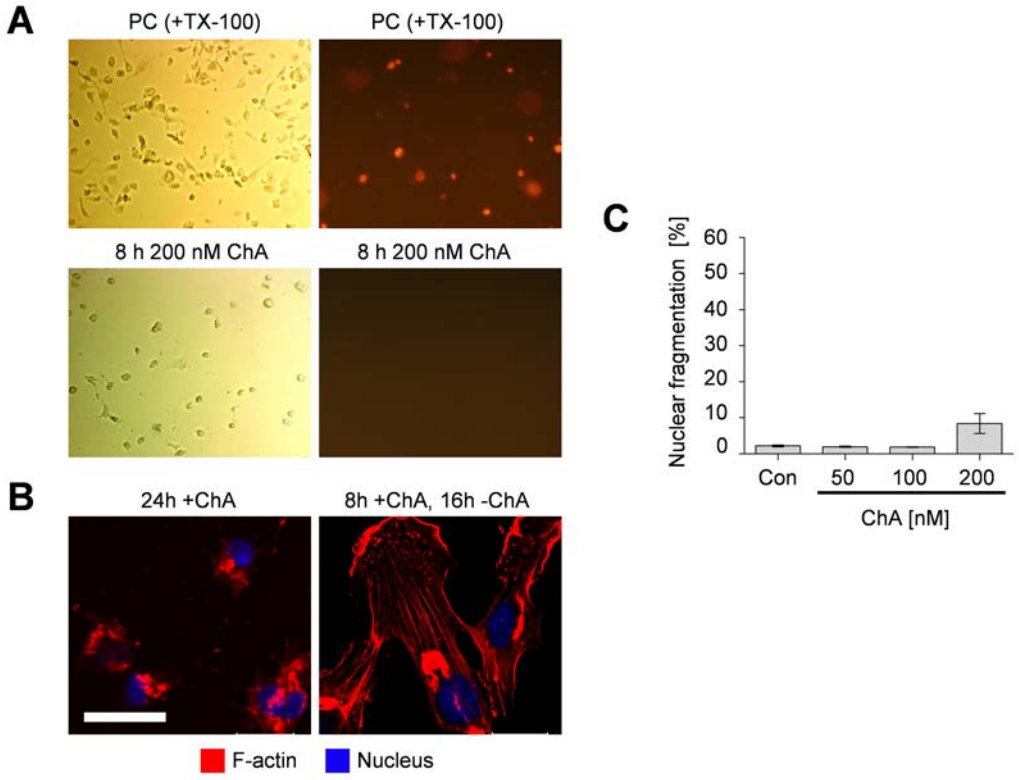

Figure 3.8: **Cells condensated after Chondramide treatment are still viable.** A: The cell membrane of condensated cells is still intact. Chondramide treated HMEC-1 were stained with propidium iodide (right images). Cells treated with Triton X-100 (TX-100) served as positive control (PC). B: Condensated HMEC-1 recover after removal of Chondramide. HMEC-1 were treated with ChA for 24 h (left) or ChA was removed after 8 h and incubated for further 16 h without ChA (right). Scale bar represents 20 μm. C: Less than 10% of HMEC-1 undergo nuclear fragmentation after cellular condensation. HMEC-1 were treated with indicated concentrations for 48 h, stained with propidium iodide and the percentage of nuclear fragmentation was measured.

Following the aggregation via time lapse imaging using pLifeakt-GFP, we could see that also at 30 nM Ch aggregates arise from stress fibers after 2 to 4 h and are then transported proximally to the nucleus (Figure 3.9). This aggregate formation is time and concentration dependent (data not shown). At the same time, lamellipodia appear to be completely unaffected. Thus, 30 nM Ch leads to an aggregation of stress fibers while lamellipodia remain still unaffected.

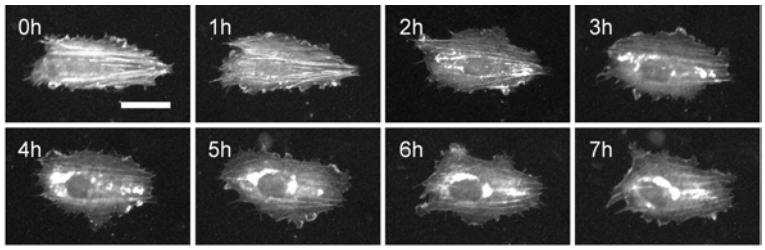

Figure 3.9: **Actin nucleation occurs at stress fibers followed by aggregate transportation to the perinuclear region.** Time lapse imaging of transfected HMEC-1 (pLifeakt-GFP) treated with 30 nM ChB for indicated time periods was performed. One representative time serie was chosen out of three independent experiments. Scale bar represents 50 μm.

In order to characterize these aggregates, we stained for markers of aggresomes, which have previously been described in connection to misfolded proteins and actin binding compounds [59, 60]. Thereby, aggresomes are located in the perinuclear region close to the microtubule organizing centre (MTOC), are not related to lysosomes or endosomes and include actin binding proteins in case of actin binding compounds.
Under Ch treatment, 80% of the cells show an aggregate in close proximity to the MTOC (Figure 3.10).

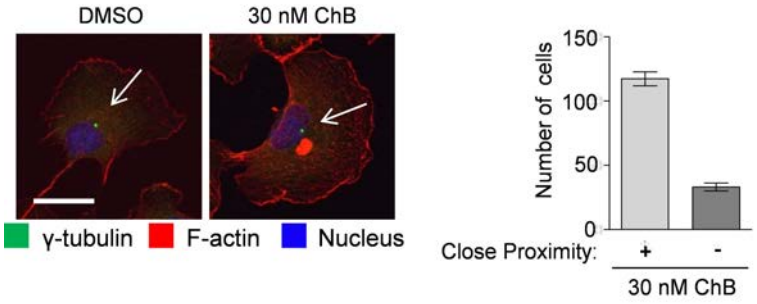

Figure 3.10: **Chondramide induced aggregates are located in proximity to the MTOC.** HMEC-1 were treated with 30 nM ChB, stained for γ-tubulin (green, white arrows) and counted. Cells were distinguished in two groups: (+) aggregates close to the MTOC or (-) not. Left: Representative images are shown. Scale bar represents 20 μm. Right: The number of cells with close proximity of aggregate and MTOC was counted (n=3).

Further, the marker for lysosomal or endosomal compartments, LAMP-1 or Rab5, respectively, were stained to check a possible localization. However, we could see no overlap in-

dicating neither a lysosomal nor an endosomal localization of the aggregates (Figure 3.11). Finally, staining of the two actin binding proteins p21-Arc and Cortactin showed a clear colocalization with the aggregate (Figure 3.11). These findings indicate that Ch induces aggresome formation.

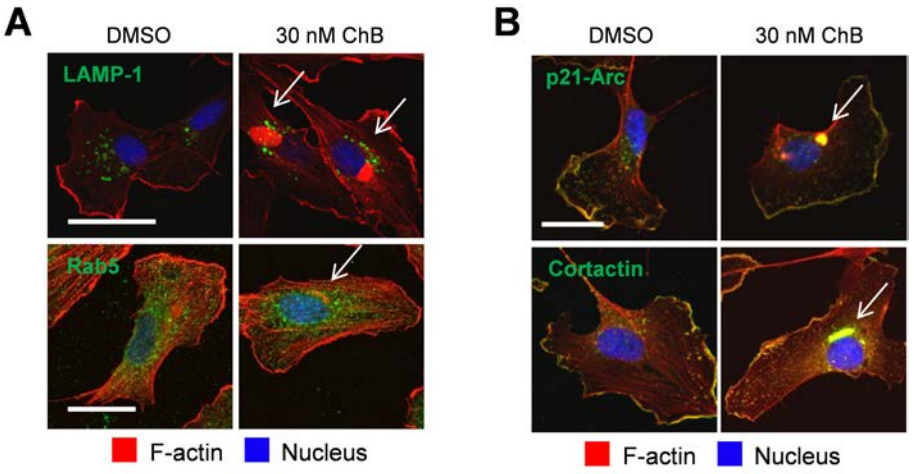

Figure 3.11: **F-actin aggregates are neither lysosomal nor endosomal and contain actin binding proteins.** A: HMEC-1 cells were stained via LAMP-1 (green) for lysosomes or Rab5 (green) for endosomes, respectively. Arrows point to aggregates. B: HMEC-1 were stained for F-actin (arrows indicate aggregates), nuclei and the actin binding proteins p21-Arc or Cortactin (green), respectively. The overlap of actin with p21-Arc or Cortactin, respectively, is shown in yellow. For all stainings, representative images were chosen out of three independent experiments. Scale bars represent 20 μm.

3.1.5 Chondramide reduces adhesion on collagen and the maturation of focal adhesions

One major step in migration and maturation of tubes is the attachment to surfaces. Thus, the influence of Ch on the adhesion of endothelial cells to ECM proteins was tested. On collagen, a clearly decreased number of cells could adhere when treated with 100 nM Ch, whereas on fibronectin no change in cell number could be seen (Figure 3.12 A). However, for both substrates, cells were not able to spread and showed a complete globular form at 100 nM (Figure 3.12 B, C). Additionally, half of the cells adhering on fibronectin showed an irregular shape meaning disturbed spreading. So, obviously, Ch can reduce on the one hand adhesion of cells to collagen and on the other hand also affects spreading on both matrices.

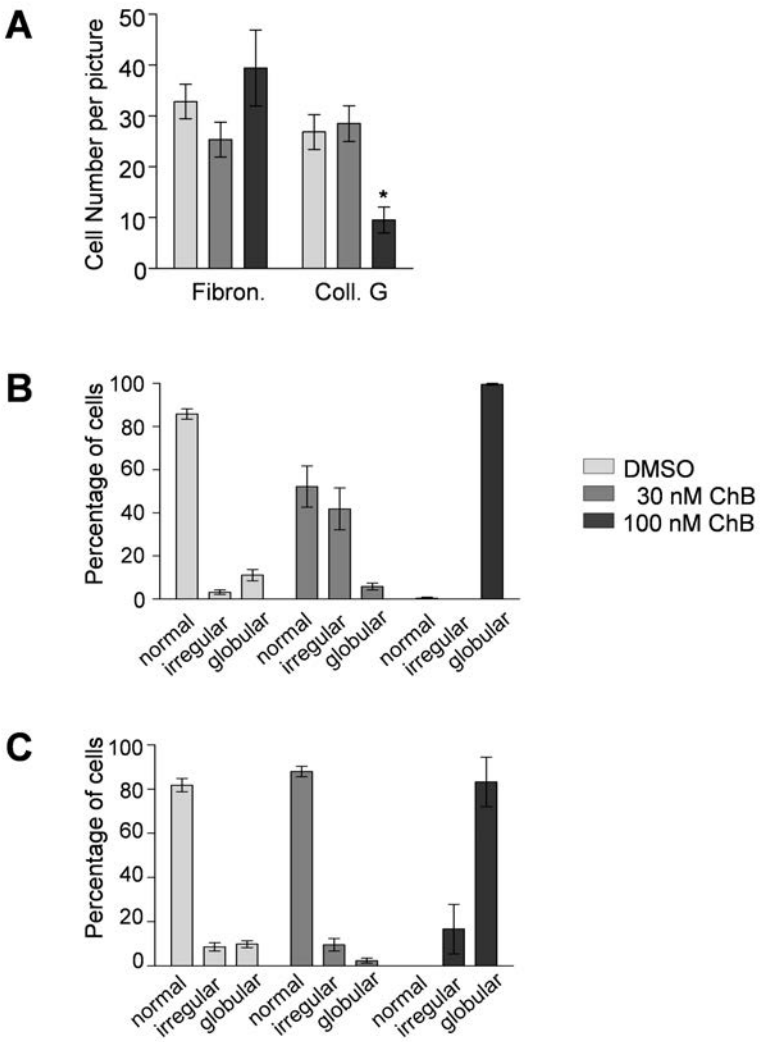

Figure 3.12: **Chondramide reduces adhesion on collagen and spreading of endothelial cells.** A: HUVECs were pretreated with ChB and seeded on fibronectin or collagen, respectively. After 30 min adhesion, cells were fixed, stained and counted on four images per sample and experiment (One-way ANOVA, Tukey post-test, * $p<0.05$, n=3). B,C: Chondramide treated cells cannot spread after attachment on fibronectin (B) and collagen G (C). Images were counted for normal spreading cells (normal), irregular shaped cells, showing non-symmetrical spreading (irregular), and completely rounded cells (globular), (n=3).

To elucidate this in more detail, we analyzed whether Ch influences integrins. Typical integrins for both substrates, $\alpha 5$ for fibronectin and $\alpha 2\beta 1$ for collagen, were stained in Ch treated cells (Figure 3.13). Thereby, 30 nM were chosen as cells at 100 nM did not adhere or

were completely rounded. We could see for both substrates that cells showed less integrin stainings at the end of stress fibers (arrows). This indicates that accumulations of integrins at stress fibers representing mature focal adhesions are reduced in Ch treated cells.

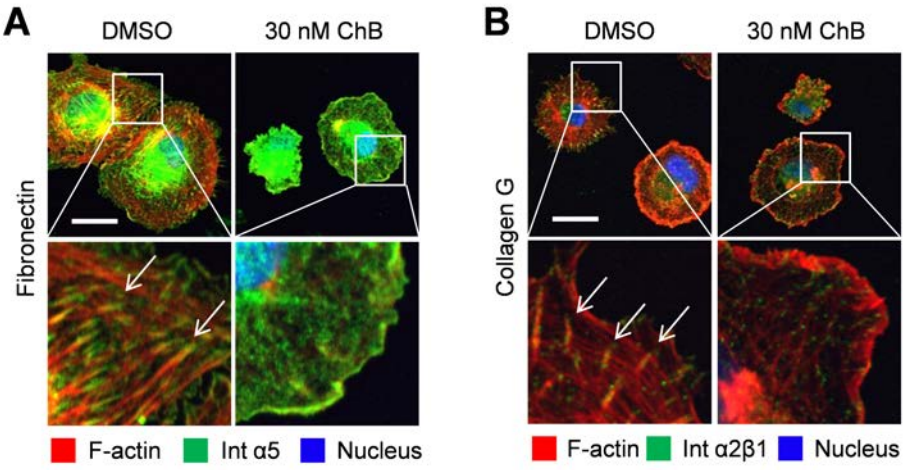

Figure 3.13: **Chondramide disturbs the maturation of focal adhesions.** Samples were stained for the fibronectin specific integrin $\alpha 5$ (left) and the collagen specific integrin $\alpha 2\beta 1$ (right), as well as actin and nuclei. Arrows indicate accumulation of integrins representing major focal adhesions. Representative images are shown. Bars represent 20 μm (n=3).

3.1.6 Chondramide affects integrin associated signaling by inhibiting Src activity

Focal adhesions play a major role in migratory signaling. Since these were influenced by Ch, we analyzed downstream signaling pathways. First, FACS analysis on total and active integrin $\beta 1$ was performed (Figure 3.14). Both active and inactive integrin $\beta 1$ were less present at the cell surface under Ch treatment hinting towards a trafficking problem but not a problem of integrin activation.

Next, the major downstream complex consisting of FAK and Src was tested on its activity via the phosphorylation statuses of its components. The autophosphorylation site Y397 of FAK was unchanged under Ch treatment (Figure 3.15). However, the Src autophosphorylation at Y416 showed less phosphorylation after incubation with Ch. Finally, the Src-dependent phosphorylation of the FAK (Y576/577) was tested and showed less phosphorylation after Ch treatment. These data indicate a reduction in the activity of the Src kinase upon Ch treat-

ment.

The inhibition of Src using the specific inhibitor Saracatenib reduced the migration of endothelial cells down to 60% at 10 μM (Figure 3.16 A). At the same concentration, the autophosphorylation of Src at Y416 is reduced (Figure 3.16 B) indicating its importance for migration.

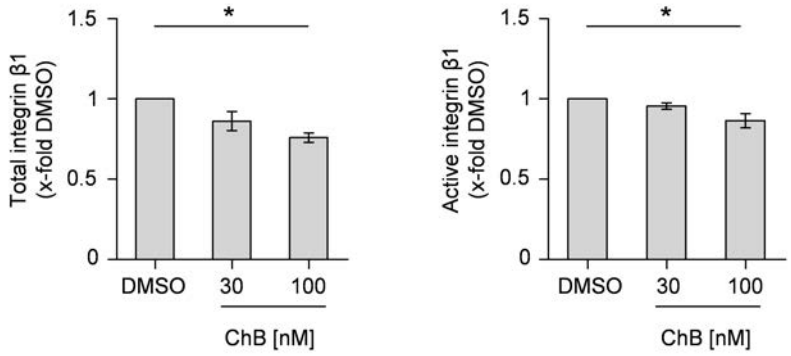

Figure 3.14: **Chondramide reduces total and active β1 integrin on the cell surface.** HUVECs were pretreated with ChB (4 h) and harvested for FACS-analysis (One-way ANOVA, Tukey post-test, * p<0.05, n=3). Conducted by D. Bartel.

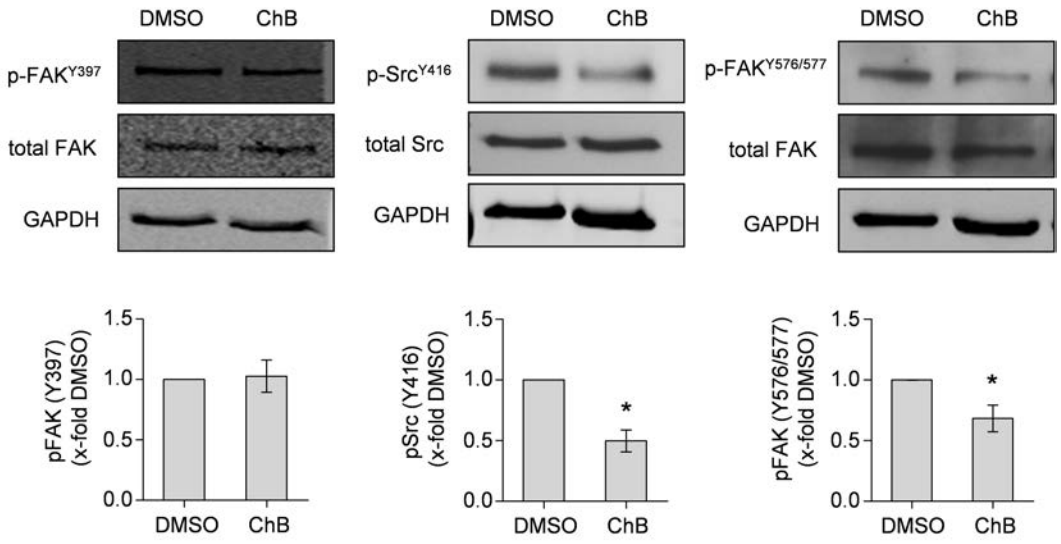

Figure 3.15: **Chondramide reduces Src activity.** HUVECs were pretreated with ChB (4 h, 30 nM), seeded freshly and harvested for Western blot analysis. Upper panel: Representative Western blot images are shown. Lower panel: Densitometric analysis of Western blots. One-way ANOVA, Tukey post-test, * p<0.05, n=3. Conducted by D. Bartel.

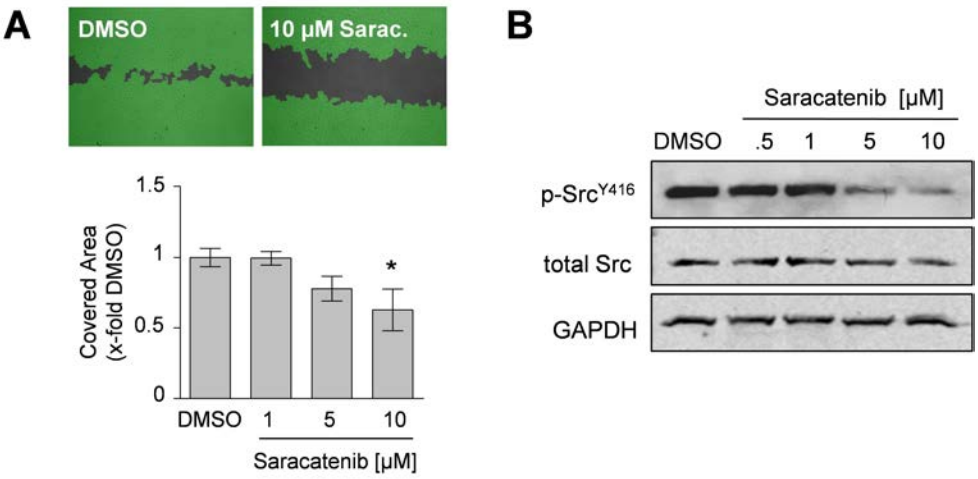

Figure 3.16: **Specific inhibition of Src using Saracatenib reduces migration of HUVECs.** A: Upper panel: Representative images of scratch assay are shown. The area covered with cells is displayed in green. Lower panel: Images were analyzed on cell covered area. (One-way ANOVA, Tukey post-test, * $p<0.05$, n=3). B: Western blot of Saracatenib treated HUVECs for pY416-Src and tot-Src are shown. GAPDH serves as loading control (n=1).

3.1.7 Chondramide reduces Rho GTPase activity

The FAK/Src complex regulates the activity of the RhoGTPases Rac1 and Rho. To test whether their activity is reduced by Ch, pull down assays were performed (Figure 3.17). Both Rac1 and Rho showed reduced activity upon Ch treatment.
Concomitant with that, the downstream target to Rho, MLC2, showed less phosphorylation at S19 as seen in Western blot and fluorescent staining (Figure 3.18). Thus, targeting the actin cytoskeleton has an effect on the upstream effectors of active Rac1 and Rho.

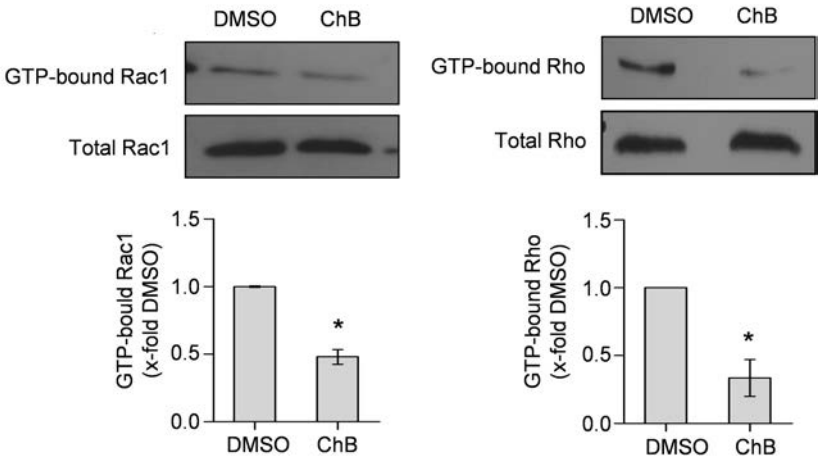

Figure 3.17: **Chondramide reduces the amount of GTP-bound Rac1 and Rho.** HUVECs were pretreated with ChB (4 h, 30 nM), seeded freshly and harvested for pull down assay. Upper panel: Representative Western blot images are shown. Lower panel: Densitometric analysis of Western blots. One-way ANOVA, Tukey post-test, * $p<0.05$, n=3. Rho pull down was conducted by D. Bartel.

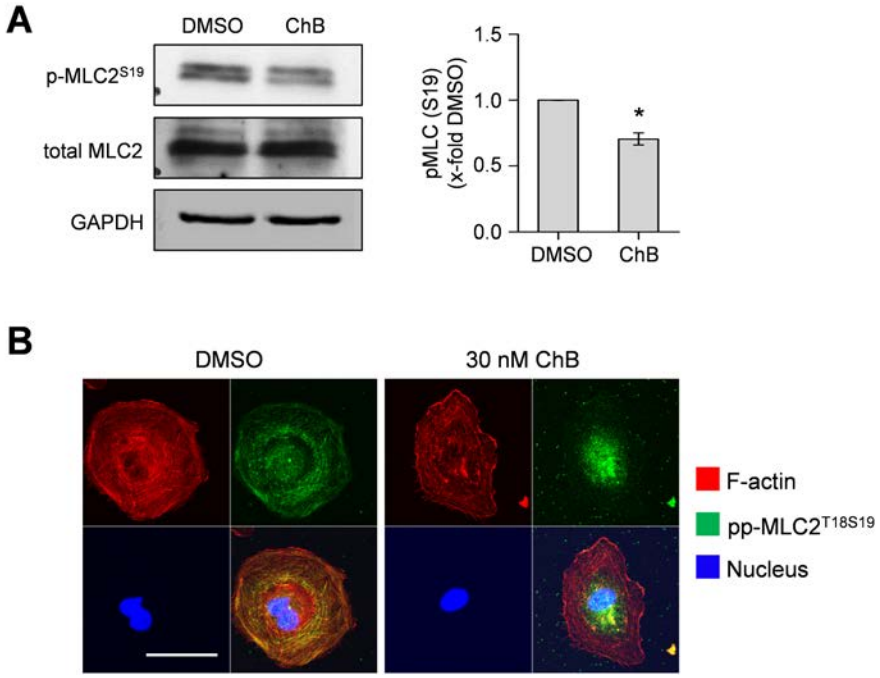

Figure 3.18: **Treatment with Chondramide reduces MLC2 phosphorylation.** A: Western blot of Ch treated HUVECs (4 h, 30 nM) for pS19-MLC2 and tot-MLC2 are shown. GAPDH serves as loading control. Left panel: Representative Western blot images are shown. Right panel: Densitometric analysis of Western blots. One-way ANOVA, Tukey post-test, * $p<0.05$, n=3. B: Fluorescent stainings of Ch treated HUVECs are shown. Cells were stained for F-actin, nuclei and ppT18S19-MLC2 (n=3). Scale bar represents 50 μm. Conducted by D.Bartel.

3.1.8 Chondramide diminishes angiogenesis *in vivo*

Finally, the *in vivo* effect of Ch on tumor vasculature was evaluated. In a murine xenograft tumor model with MDA-MB-231 cells, Ch treatment led to a significantly reduced tumor weight [61]. These tumors were used to analyze the degree in vascularization of treated and untreated tumors. Stainings of tumors for CD31 revealed a significant reduction of the microvessel density in Ch treated tumors (Figure 3.19).

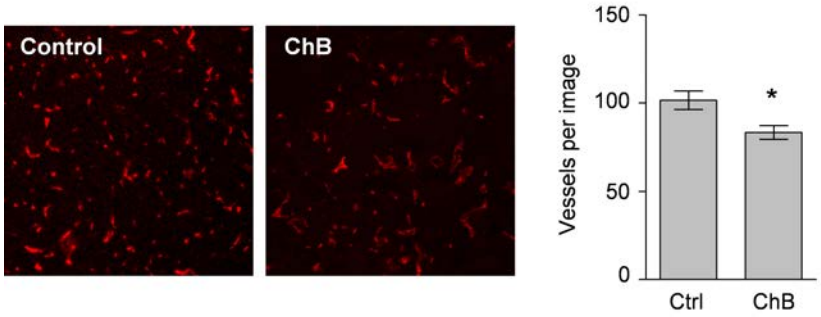

Figure 3.19: **Chondramide reduces tumor angiogenesis *in vivo*.** 10 mice per group with subcutane tumors were treated thrice a week with Chondramide or solvent *i.p.* for 34 days. Harvested tumors were stained for CD31 (left panel). Four images per tumor (10x objective) were taken and vessels were counted. (40 images per group, t-test, unpaired, * $p<0.05$).

3.2 Chondramide inhibits metastasis *in vitro* and *in vivo*

3.2.1 Chondramide diminishes metastasis *in vivo*

First, we evaluated the pharmacological, anti-metastatic potential of Chondramide (Ch) *in vivo*. To this end, a 4T1-Luc metastatic mouse breast cancer model was used [62, 63, 64]. Hereby, a murine 4T1-Luc mammary cancer cell line expressing recombinant luciferase is injected intravenously in BALB/cBγJRj mice. These luciferase expressing cancer cells metastasize to the lung and can be detected via bioluminescent measurement. Experiments were conducted by L. Schreiner [65] and R. Kubisch.

The evaluation of the bioluminescent signal in the lungs of untreated and Ch treated mice revealed a significant reduction of metastasis for Ch treated mice compared to control mice (Figure 3.20 A, B). Over the treatment period, the weight of Ch treated mice stayed constant indicating a good tolerance of 0.5 mg/kg Ch during application (Figure 3.20 C).

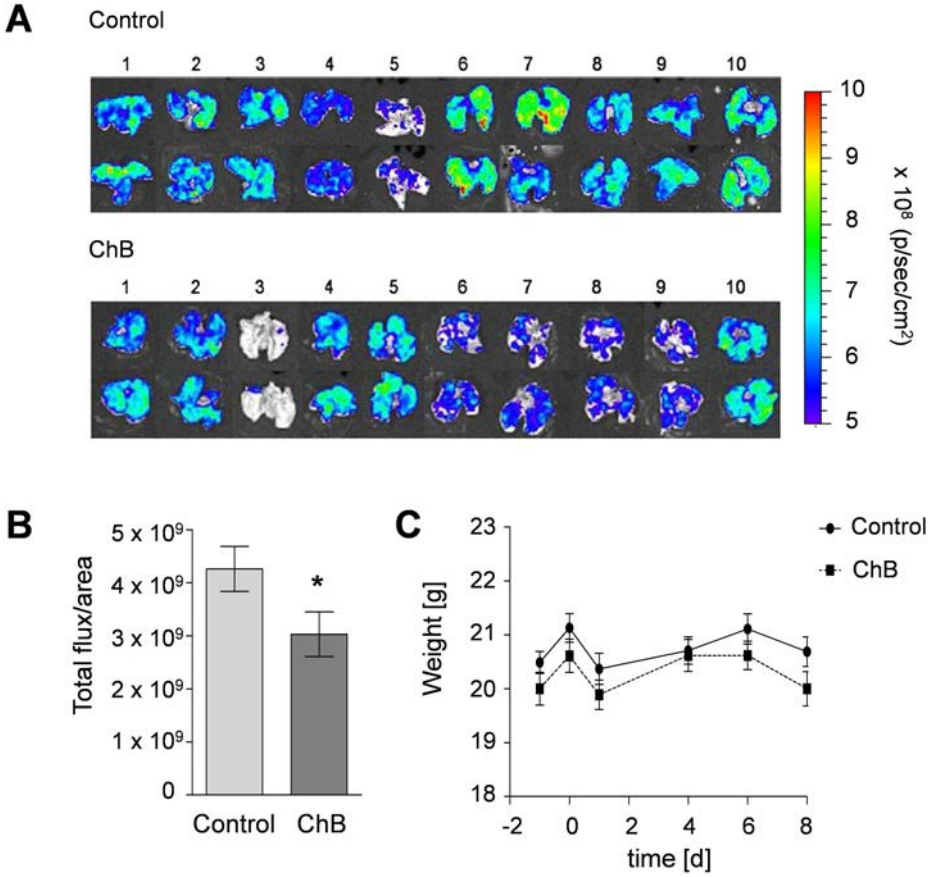

Figure 3.20: **Chondramide reduces metastasis *in vivo*.** 1 x 10^5 4T1-Luc cells were injected intravenously into pretreated (0.5 mg/kg ChB) and untreated BALB/cBγJRj mice. A: 8 days after cell inoculation mice were sacrificed, lungs harvested and used for recording bioluminescence signals. Each lung was imaged from the dorsal (upper panel) and ventral (lower panel) side. Color bar scales were equalized. B: Quantitative evaluation of metastasis to the lungs. Regions of interest were defined (ROI) and total luciferin signal in ROIs was calculated as photons/second/cm^2 (total flux/area). Bars represent the mean $\pm$ SEM of ten lungs per group. * $p<0.05$ (t-test). C: Mouse weight over treatment period. Weight of treated (ChB) and untreated (DMSO) from day of cell inoculation (day 0) to euthanasia (day 8) is shown as the mean $\pm$ SEM for each group. Conducted by L. Schreiner [65] and R. Kubisch.

3.2.2 Chondramide reduces migration of highly invasive cancer cells

Based on this promising result, the activity of Ch on cancer cell metastasis was evaluated *in vitro*. In a first trial, the effect of Ch on cancer cell migration was tested with several cancer cell lines. To this end, the cell lines MCF-7 and L3.6pl as well the cell lines HUH-7 and MDA-MB-231 were tested in scratch-assay. The migration of MCF-7 and L3.6pl cells was only reduced at 200 nM ChA. In contrast, the migration of the more invasive cells HUH-7 was inhibited to 70 or 50% at 50 or 200 nM Ch, respectively, and the highly invasive cell line MDA-MB-231 was inhibited in a concentration dependent manner up to less than 50% at 200 nM (Figure 3.21). As a model for highly invasive cancer cells the cell line MDA-MB-231 was used for further experiments.

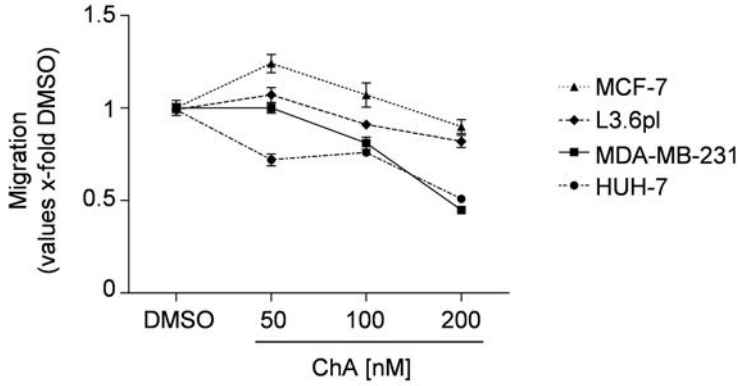

Figure 3.21: **Chondramide inhibits cell migration of several cancer cell lines.** Cancer cells were allowed to migrate in scratch assay at indicated concentrations of Chondramide (n=3).

3.2.3 Chondramide inhibits FCS induced migration and invasion *in vitro*

Next, the inhibitory effect on FCS induced migration was tested. For this purpose, MDA-MB-231 were tested in Boyden chamber assay. The migration could be inhibited significantly by Ch at 30 or 100 nM down to 60 or 70%, respectively (Figure 3.22 A). To study the effect of Ch on invasiveness, matrigel filled Boyden chambers were used. Here, Ch inhibited cell invasion at 30 nM and 100 nM to less than 50% (Figure 3.22 B).

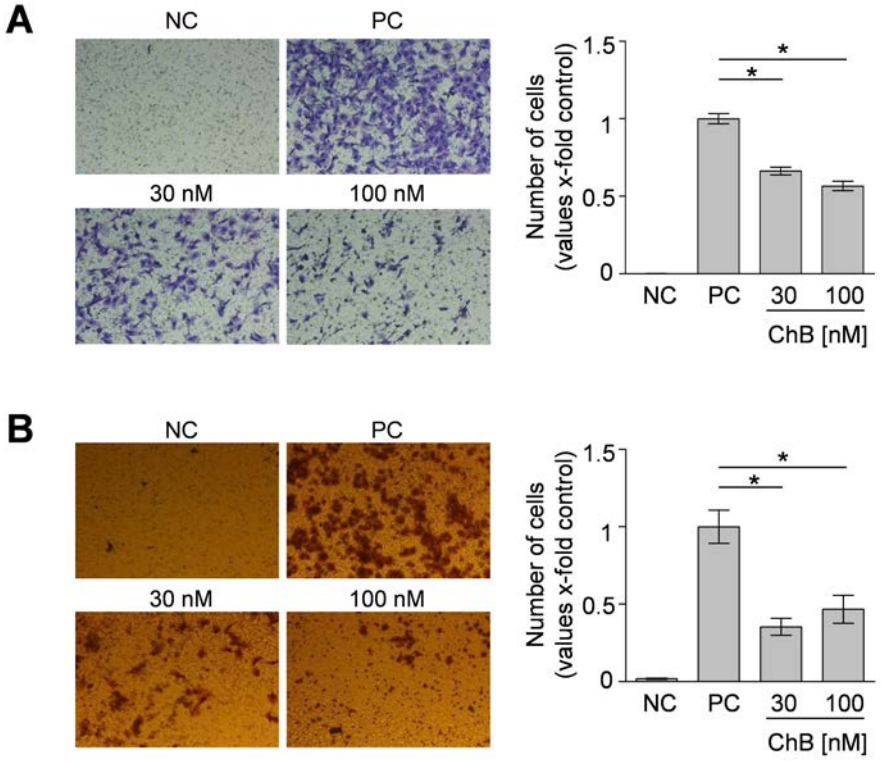

Figure 3.22: **Treatment with Chondramide reduces breast cancer cell migration and invasion.** A: Chondramide treated and untreated MDA-MB-231 cells were allowed to migrate in Boyden chamber for 16 h. B: Chondramide inhibits invasion of MDA-MB-231 cells through matrigel in Boyden chamber (48 h). A,B: For positive control (PC) lower compartment was filled with medium plus 10% FCS, for negative control (NC) only medium without FCS was added. Bars indicate migration relative to PC. * $p<0.05$ One-way ANOVA,Tukey post-test, n=3.

3.2.4 Chondramide reduces adhesion of MDA-MB-231 cells on several surfaces

In order to further elucidate the effect of Ch on cell migration, the important step in migration, cell adhesion, was tested. Here, Ch reduced the attachment of cells to several matrices at 100 nM, however, not at 30 nM (Figure 3.23 A). This indicates, that anti-adhesive properties of Ch can contribute to an anti-migratory effect, however, this seems not to be the only factor diminishing cancer cell migration. Fluorescent stainings of the adhering cells revealed that cells treated with 30 nM Ch showed normal cell morphology whereas the few adhering cells at 100 nM Ch were not able to spread (Figure 3.23 B).

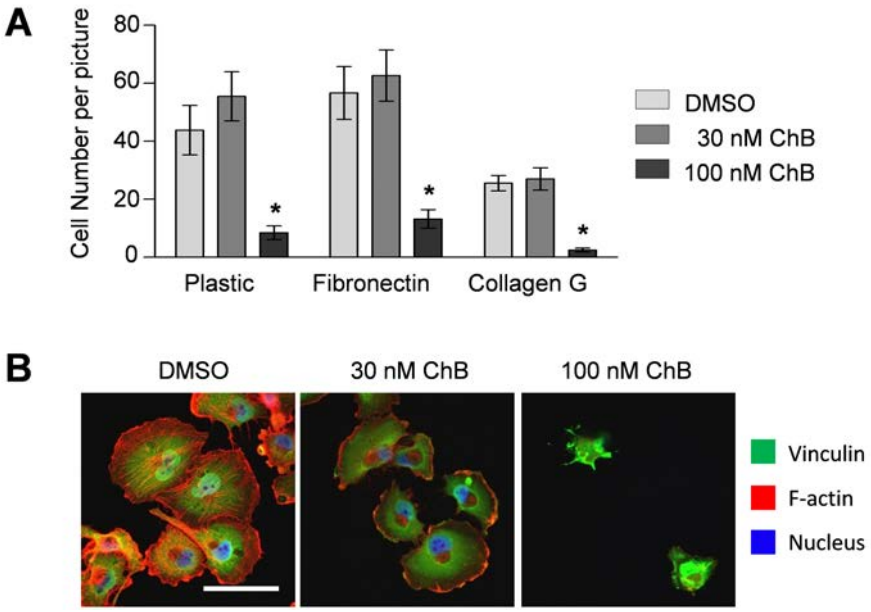

Figure 3.23: **Chondramide inhibits adhesion and spreading of MDA-MB-231 cells.** A: Pretreated MDA-MB-231 cells were seeded freshly on different surfaces and counted after fixation. * $p<0.05$ One-way ANOVA, Tukey post-test, n=3. B: Cells from A were stained for F-actin, nuclei and Vinculin. Bar represents 50 μm.

3.2.5 Chondramide affects stress fibers of MDA-MB-231 cells

To get a first insight into the intracellular processes upon Ch treatment, the actin cytoskeleton of MDA-MB-231 cells was stained. Thereby, we observed thinner stress fibers compared to control and aggregation close to the nucleus after 4 and 8 h (Figure 3.24 A). After 24 h the cells were completely condensed. These condensed cells recovered to total cell size after substance removal like endothelial cells indicating their viability (Figure 3.24 B).

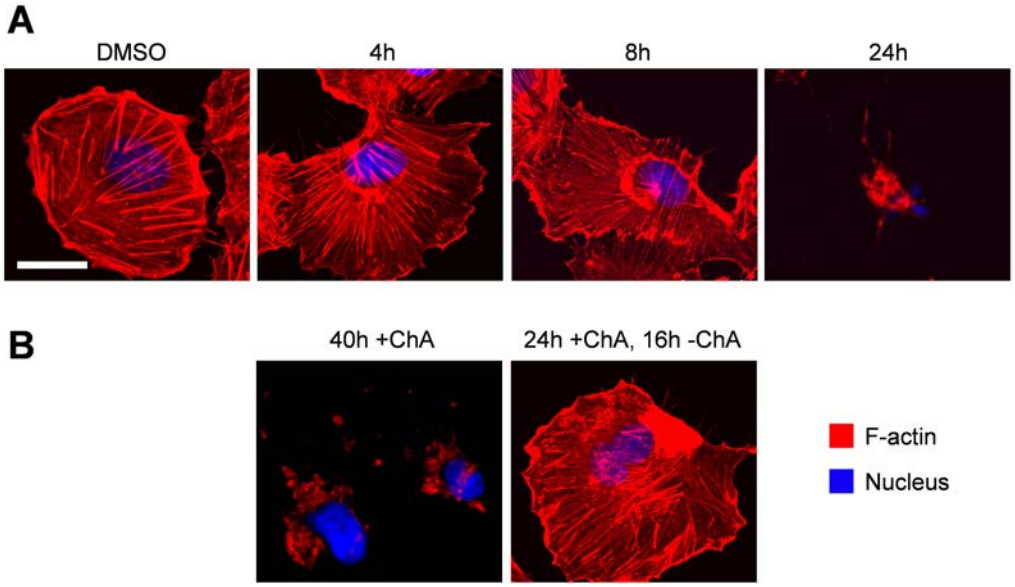

Figure 3.24: **Chondramide leads to reduction of stress fibers and F-actin aggregation.** A: MDA-MB-231 cells were treated with 200 nM ChA or DMSO for indicated time periods, fixed and stained for F-actin and nuclei. B: Removal of Ch allows cells to recover to normal cell size. Bar represents 20 μm.

3.2.6 Chondramide reduces the activity of the RhoGTPase Rho but not Rac1

To investigate whether stress fiber reduction seen in figure 3.24 is a direct effect of Ch or induced due to alterations in signaling, the upstream effectors of the actin-cytoskeleton were tested on their activity. Therefore, the RhoGTPases Rac1 and Rho were analyzed using pull down assay. Hereby, we could see no alterations in the amount of GTP-bound Rac1 (Figure 3.25 A). However, the level of GTP-bound Rho was clearly reduced at 30 nM Ch (Figure 3.25 B). The reduced activity of Rho could be confirmed further downstream as the regulatory myosin light chain 2 (MLC2) was less phosphorylated at Ser19 (Figure 3.25 C).

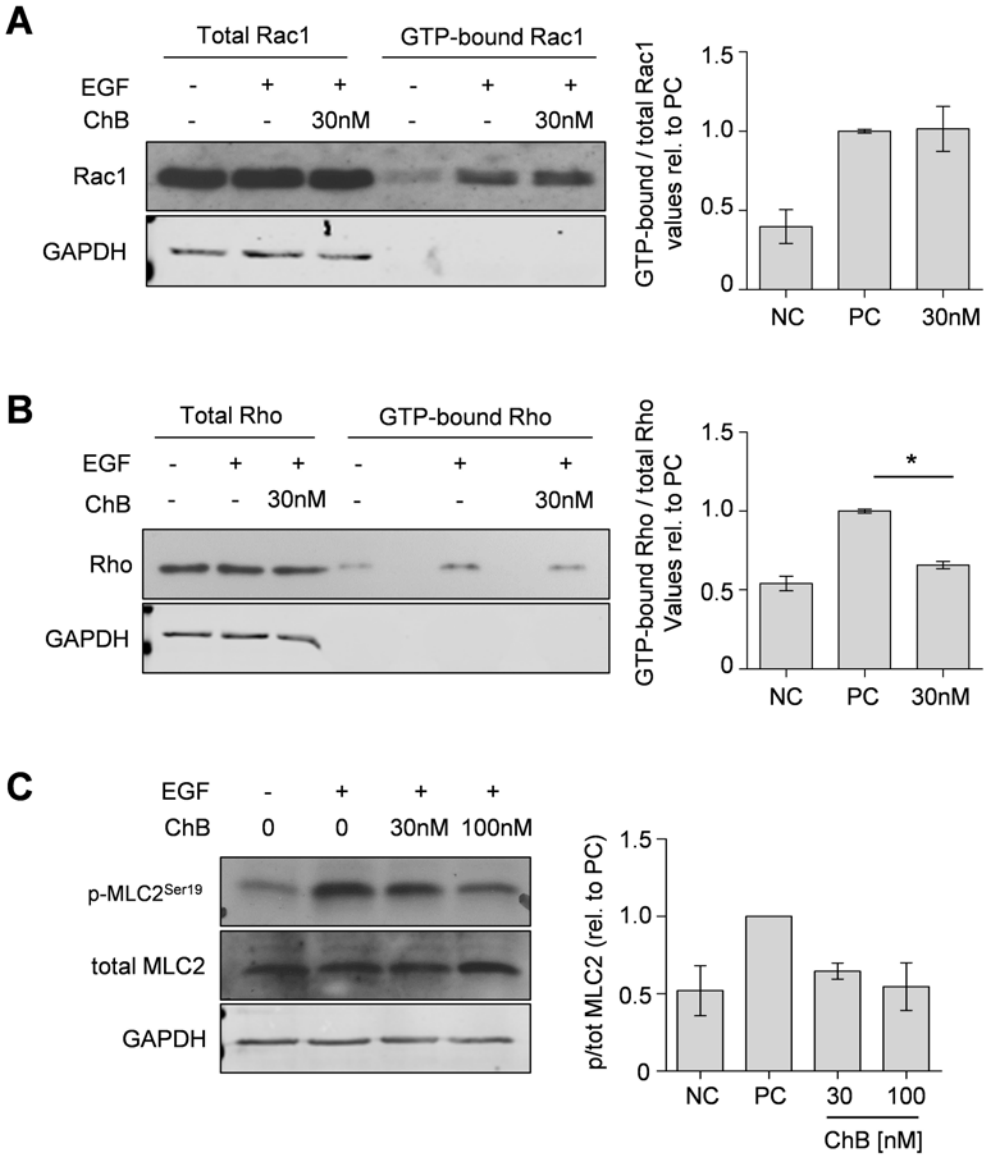

Figure 3.25: **Chondramide affects activation of the RhoGTPase Rho.** A: Rac1 pull down was performed for untreated and ChB treated cells upon EGF stimulation (5 min). B: After same treatment a Rho pull down was conducted. C: Myosin light chain 2 (MLC2) was analyzed on its activation state via Western blot analysis upon EGF stimulation (5 min). Bars represent mean ± SEM. * $p<0.05$ One-way ANOVA, Tukey post-test, n=3. A,B,C: Left panel: One representative Western blot is shown. Right panel: Densitometric analysis of Western blots.

3.2.7 Chondramide has no effect on the activation of the EGF-receptor and downstream signaling

Further, the reason for the reduced Rho activity should be evaluated. As the RhoGTPases were activated through extracellular EGF stimulation in these experiments, we tested the EGF-receptor (EGFR) on its ability for autophosphorylation. The autophosphorylation at Y1068 of the EGFR was not affected by Ch treatment (Figure 3.26). Neither 30 or 100 nM Ch nor a very short or longer time point showed any changes in the phosphorylation state. Concomitant with that, the phosphorylation status of the downstream effectors to EGFR, Akt and Erk, at S473 or T202/Y204, respectively, showed no effect of Ch treatment compared to positive control (Figure 3.26). This data indicates normal activation of these pathways under Ch treatment.

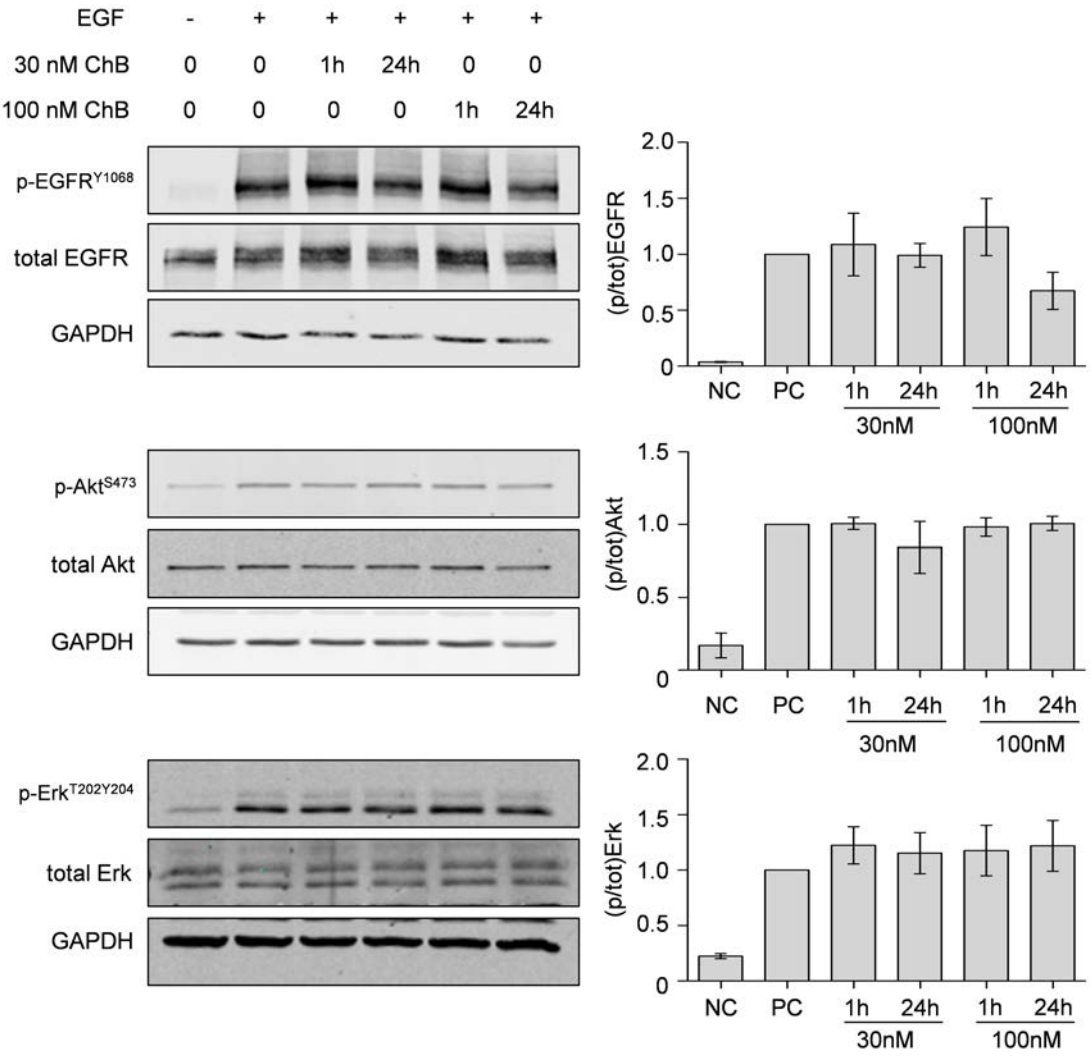

Figure 3.26: **Chondramide does not influence EGFR signaling.** MDA-MB-231 cells were treated with Ch (1 or 24 h), stimulated with EGF (5 min) and analyzed via Western blot analysis on EGFR, Akt and Erk. Left panel: One representative Western blot is shown. Right: Densitometric analysis of Western blots. * $p<0.05$ One-way ANOVA, Tukey post-test, n=3.

3.2.8 Chondramide diminishes cellular contractility

The activation of the RhoGTPase Rho can also occur due to intra- or extracellular forces. One guanine nucleotide exchange factor (GEF) that is known to be activated by force and to activate RhoA in MDA-MB-231 cells is Vav2. In fact, the activity dependent phosphorylation site Y172 of Vav2 was less phosphorylated under Ch treatment (Figure 3.27).

To finally see whether cellular force is reduced under Ch treatment, we tested the ability of MDA-MB-231 cells to exert contractile force. Cellular force on surrounding matrix can be visualized as exerted forces result in matrix movement which can be imaged by embedded fluorescent beads [66, 56]. To this end, cells were embedded in matrigel containing fluorescent beads and images were taken over 4 h. Control cells revealed a clear contractile force on the surrounding matrix as seen by bead movement towards the cell (Figure 3.28 A). This bead movement was reduced at 30 nM and even more at 100 nM (Figure 3.28 B). This data indicates a significant reduction of intracellular originating force in cells treated with Ch.

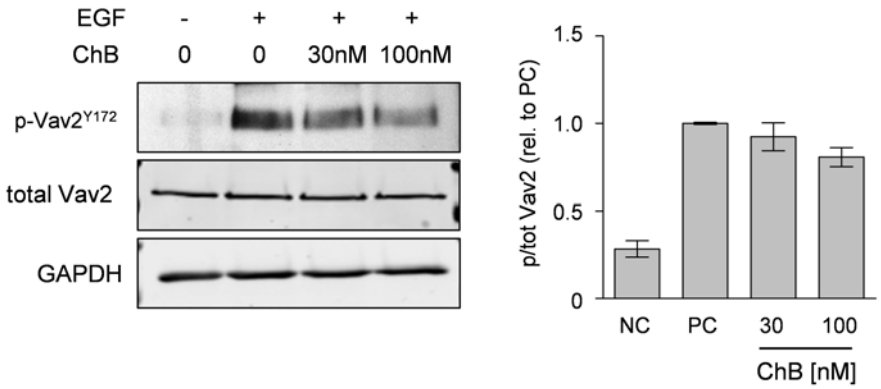

Figure 3.27: **Phosphorylation of the Rho-GEF Vav2 is reduced by Chondramide.** Phosphorylation of Vav2 at Y172 was tested via Western blot analysis upon EGF stimulation. Left panel: One representative Western blot is shown. Right: Densitometric analysis of Western blots. (n=3)

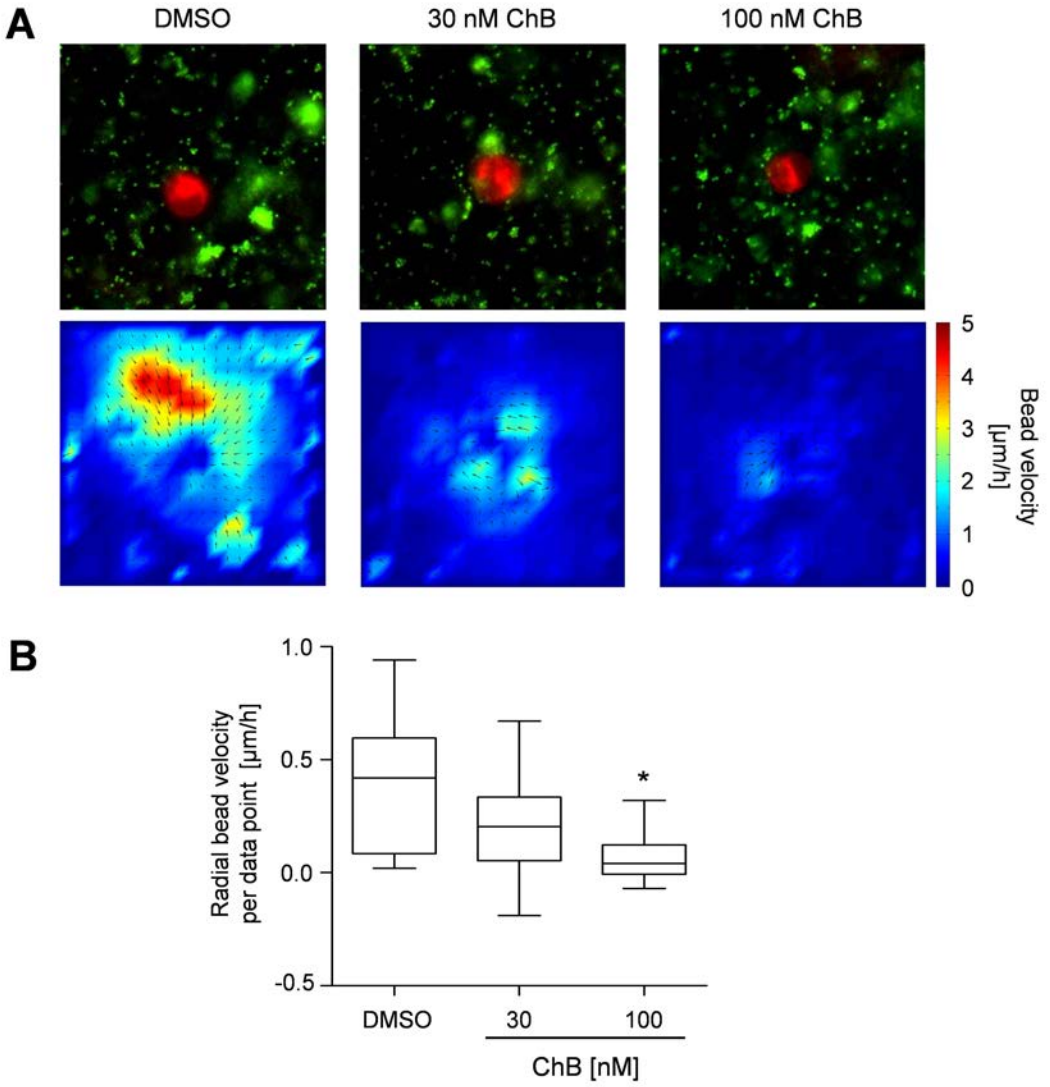

Figure 3.28: **Chondramide diminishes cellular contractility.** A: MDA-MB-231 cells were pretreated for 24 h as indicated, stained with CellTracker^{TM}Red, embedded in matrigel containing fluorescent beads and pictures were taken over 4 h every 15 min. Cellular, contractile force on the surrounding matrix was visualized via bead movement towards the cell and analyzed using PIV analysis. Upper panel: Representative images of cells (red) and fluorescent beads (green) t=0. Lower panel: PIV analysis of bead velocity in the 2D projection. Color codes show bead velocity indicating applied force. Direction of vectors indicates averaged direction of bead movement. B: For quantitative analysis the radial velocity (bead velocity towards the cell center) per data point was calculated. Minimum 13 cells per condition were analyzed. * $p<0.05$ One-way ANOVA, Tukey post-test.

4: Discussion

The cytoskeleton is an attractive target in cancer therapy as proven by the treatment of cancer with microtubule disturbing drugs. In the evaluation of actin binding compounds performed in the 70s and 80s, targeting the actin cytoskeleton was assessed as too toxic for clinical application [67, 9, 10]. However, since then, new actin binding compounds were discovered, that could reveal different properties to those first tested, and new possibilities are established for directed targeting of chemical compounds to their site of action. These developments rise the interest in actin targeting compounds in cancer treatment again. Nevertheless, functional and mechanistic studies concerning cancer treatment with actin targeting compounds are rare now due to their negation in the last centuries. Especially, oncogenic processes dependent on the actin cytoskeleton are worthwhile to test [68]. Thus, the migration dependent processes, tumor angiogenesis or tumor metastasis, are attractive to target with an actin binding compound.

4.1 Chondramide as anti-angiogenic agent

4.1.1 Actin targeting in anti-angiogenic therapy

Regarding angiogenesis, investigations targeting the actin cytoskeleton directly to inhibit the process of blood vessel formation are relatively rare. Among them, the actin destabilizer Cytochalasin D was shown *in vitro* to inhibit cell growth, migration and tube formation [69] of endothelial cells as well as to diminish angiogenesis in a chorioallantoic membrane (CAM) assay [70]. For Latrunculin, its derivative 15-O-methyllatrunculin B showed promising anti-angiogenic activity in a CAM assay [71]. To our knowledge, the actin nucleating compound Jasplakinolide has never been tested for potential anti-angiogenic effects possibly due to high toxicity *in vivo* [10, 72]. Thus, actin binding compounds have not been

investigated in detail concerning their mechanism of action and potency in angiogenic therapy.

This study shows promising anti-angiogenic effects of Chondramide *in vitro* and *in vivo*. In fact, we could show a pharmacological reduction of tumor blood vessels *in vivo* at a non-toxic concentration. Furthermore, we could demonstrate that major hallmarks of angiogenesis [29], namely the proliferation, the migration and the *in vitro* tube formation of endothelial cells, are inhibited by Chondramide in a low nanomolar range.

4.1.2 Chondramide induces aggresome formation

Intracellularly, the most obvious effect of Chondramide in endothelial cells potentially causing the anti-migratory effect is the aggregation of fibrilous actin. This observation is in line with another study applying Chondramide in Pt K2 potoroo cells [26] and is also known for other actin binding substances [60]. These actin toxin induced lumps are called aggresomes, a cellular stress response to missfolded proteins [59]. Criteria for aggresomes are the localisation close to the MTOC and for actin toxins the inclusion of actin binding proteins [73, 74]. These features are shared with the Chondramide induced aggregates revealing those as aggresomes. Thus, Chondramide induces aggresomes as a stress response in endothelial cells.

4.1.3 Chondramide reduces stress fibers potentially diminishing focal adhesion maturation

The aggregation of actin by Chondramide is first seen at stress fibers and results in a disintegration of these fibres. This is in accordance with findings for Jasplakinolide [74] as well as fluorescently labeled Chondramide which preferentially stained stress fibers [27]. The functionality of stress fibers, however, is important for further structures in the cell. So, functional contractility from stress fibers is needed for the maturation of focal adhesions in endothelial cells [75]. Thus, we propose the disintegration of stress fibers as the reason for impaired maturation of focal adhesions observed after Chondramide treatment. In addition to this, the reduced amount of integrins at the cell surface may contribute to fewer focal adhesions.

4.1.4 Chondramide diminishes signal transduction at focal adhesions and downstream signaling

Focal adhesions represent a major platform for integrin outside-in signaling, which is important in spreading and migration [45]. Consequently, the disturbance of these adhesive structures has a striking impact on important signaling pathways for migration. One central complex in this signaling cascade is built by the focal adhesion kinase (FAK) and Src. Under Chondramide treatment, the autophosphorylation of Src at Y416, needed for its own activation [76], and the Src dependent phosphorylation of FAK at Y576/577 [77] are reduced. Both phosphorylation sites are an indication of reduced Src activity. Interestingly, it has been reported that the translocation of Src to focal adhesions is actin dependent in swiss 3T3 cells [78, 79]. Thus, in addition to a reduced activation of Src due to less integrins, the translocation to the membrane and FAK could be impaired resulting in a reduced autophosphorylation. This could also explain why the autophosphorylation of Src but not the one of FAK is disturbed. Most importantly, the inhibition of Src yielded in reduced migration of endothelial cells. This Src dependent inhibition reveals the importance of Src activity for endothelial cell migration.

Corresponding to a reduced activity of Src and, thus, the whole complex FAK/Src, further downstream signaling would be expected to be diminished [45]. Indeed, the downstream activated RhoGTPase Rac1 is reduced in activity at same conditions like Src. Although the FAK/Src complex mediates a transient inhibition of Rho activity, a later Src-dependent Rho activation is discussed [45]. This activation of Rho is supposed to initiate after the spreading phase due to mechanical stimuli and could be reduced under Chondramide treatment as Chondramide treated cells showed defects in spreading, and finally, lead to the lower levels in Rho-GTP. Obviously, Chondramide has an overall inhibitory effect on the RhoGTPases and thus, on very important pro-migratory signals.

4.1.5 Conclusion concerning angiogenesis

Taken together, Chondramide inhibits major pro-migratory signals via the disintegration of stress fibers, and thus, inhibits migration via two parallel ways: first, the disintegration of stress fibers itself and second, the resulting reduction in pro-migratory signals like Src and RhoGTPases (Figure 4.1).

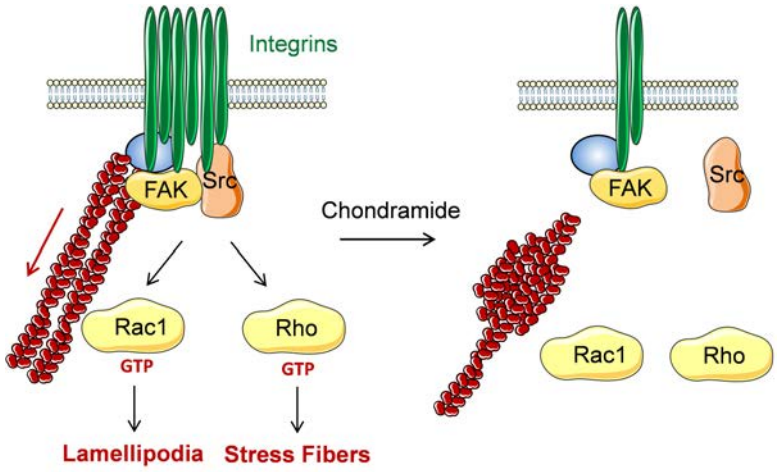

Figure 4.1: **Inhibitory effect of Chondramide in endothelial cells.** Chondramide induces actin aggregation and stress fiber solvation. As a consequence, the maturation of focal adhesion is hampered resulting in diminished complex formation of Src and FAK, finally, leading to reduced activation of RhoGTPases. Concluding, stress fiber solvation, inhibited focal adhesion maturation and RhoGTPase activity can lead to reduced cell motility, finally, inhibiting angiogenesis.

With these investigations, we show insights into the mechanism how Chondramide diminishes the migration of endothelial cells. Further, we can demonstrate that the actin polymerizing compound Chondramide inhibits angiogenesis *in vitro* and *in vivo*. This work fills the gap of an actin polymerizing compound for anti-angiogenic therapy. Most importantly, it supports the idea of targeting actin in anti-angiogenic therapies and reveals Chondramide as an interesting structure for further development.

4.2 Chondramide as anti-metastatic compound

The formation of metastasis is the major cause of death in cancer diseases [31]. However, treatments targeting invasive cells are missing. With Chondramide we tested the anti-metastatic potential of an actin targeting agent against invasive breast cancer cells.

4.2.1 Chondramide impairs cellular contractility in amoeboid cell migration

During invasion, cellular contractility is of utmost importance. Classic migration depends on contractility as the cell rear has to be retracted after cell protrusion and formation of new adhesions in the migration direction. Further, the amoeboid migration of cancer cells is mostly driven by contractile force depending on Rho/ROCK signaling but not proteolysis [35, 36]. The highly invasive cell line MDA-MB-231 follows the scheme of an amoeboid migration through matrigel, requiring a contractile uropod dependent on RhoA and MLC-2 activity [56]. Thereby, cells exert contractile force to the surrounding matrix resulting in matrix accumulation at the cell rear pushing the cell forward. Accordingly, we observed an amoeboid cell migration with round cell shape of MDA-MB-231 cells in matrigel and a matrix deformation shown by fluorescent bead movement. This bead displacement was abolished after Chondramide treatment indicating reduced contractile force of the cell. The invasion of MDA-MB-231 cells was inhibited under Chondramide treatment in a comparable setting like contractility indicating that impaired contractility most likely contributes to reduced invasion. Further, the observation that migration and invasion are inhibited at same concentrations of Chondramide is reasonable for amoeboid migration considering that this migration mode is independent of proteolysis but mainly driven by contractile force.

A reason for the reduced contractility could be the thinning of stress fibers after Chondramide treatment. As stress fibers were thinned in 2D and fluorescent Chondramide was shown to bind preferentially to stress fibers [27], Chondramide binding to those could affect their structure, finally, leading to reduced contractility.

4.2.2 Chondramide impairs pro-contractile signaling

Further, the signaling cascade leading to contractility, via Rho/ROCK and myosin, is known to enhance invasion when upregulated [80, 81]. Chondramide treatment diminishes the activity of Rho and MLC2. Other factors like Rac1 or EGFR and its downstream factors, Akt and Erk, were not affected at same conditions. Thus, Chondramide inhibits the pro-contractile signaling cascade quite specific.

Concerning the inhibition of Rho, a link to Chondramide is less obvious. Interestingly, a connection between contractile force and RhoA activation is reported not only from Rho being required for contractility but also the other way around that contractile force induces RhoA activation [48]. In this context, Vav2 has been shown to be induced by applied forces in the form of stretching in mesangial cells [47] and Vav2 is known to be necessary for a full activation of RhoA in MDA-MB-231 cells [82]. These observations are in line with our findings revealing that Vav2 and RhoA are less active in Chondramide treated cells potentially reducing contractility (Figure 4.2).

4.2.3 Chondramide shows anti-metastatic effects without acute toxicity

The approach to target the actin cytoskeleton has been thought to be too toxic for clinical application [10]. However, the feasibility to target actin is shown here in an *in vivo* mouse model of tumor metastasis. Herein, treatment with Chondramide diminishes the metastasis of mammary cancer cells to the lung significantly. As migration is reduced at lower concentrations and shorter time points than nuclear fragmentation occurs, we propose that the inhibitory effect on metastasis is not due to an apoptotic effect but the abrogation of migration and invasion. The dose of 0.5 mg/kg was well tolerated as the body weight of treated mice stayed constant throughout the observation period. Although there is still room for further development, e.g. specific targeting, we could show a pharmacological effect for Chondramide on metastasis *in vivo* without acute toxicity.

4.2.4 Conclusion concerning metastasis

Concluding, Chondramide most likely reduces contractility in two ways: first, via direct interaction with stress fibers and, second, via reduced intra-cellular force diminishing Rho activation.

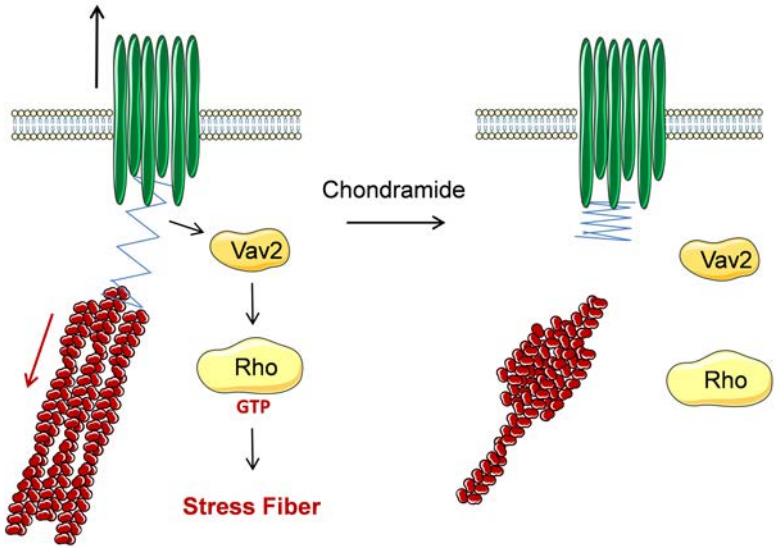

Figure 4.2: **Inhibitory effect of Chondramide in breast cancer cells.** Chondramide treatment induces the aggregation of stress fibers and diminishes cellular contractility. Consequently, the force induced GEF Vav2 as well as the downstream RhoGTPase Rho are less active further reducing contractility.

As therapies against cancer metastasis are still missing, more efforts need to be made in research addressing metastatic cancer cells. This work provides evidence that actin is a suitable target to inhibit cancer cell migration, and gives first insights into underlying mechanisms. Combining actin binding natural compounds with specific targeting strategies could lead to a powerful weapon to treat tumor metastasis.

4.3 Chondramide as a dual inhibitor of angiogenesis and metastasis

In the last century, the treatment of cancer with anti-angiogenic drugs faced the problem of limited success in clinical studies. After a initial response, tumor progression escaped from

treatment. This led to a survival benefit in the range of month but no change in the overall survival or permanent cure [83, 84, 85, 86]. Tumor escape is attributed to the establishment of resistances against anti-angiogenic therapies. One mode of response is the turning-on of alternative pro-angiogenic pathways when blocking one of those. E.g. in the treatment with Bevacizumab, a VEGF binding antibody, other angiogenic factors like EGF or platelet derived growth factor (PDGF) become upregulated [87, 88, 89]

Another mechanism of escape is the selection of aggressive cells due to hypoxic pressure [86, 90]. Via the inhibition of new blood vessel formation, reduced oxygen supply deteriorates the cellular situation in the tumor favoring motile cells able to escape this environment. In mouse models as well as in the clinic, the treatment with Bevacizumab increased the invasiveness of primary tumors [91, 92]. Also the VEGF-receptor tyrosine kinase inhibitor sunitinib induced invasiveness and metastasis [93].

In this context, the treatment with Chondramide offers a huge advantage. As we could show with our work that Chondramide interferes with both, angiogenesis and metastasis, the major side effect of pro-invasive selection could be overcome in one with the anti-angiogenic therapy.

4.4 Future perspectives

4.4.1 Treatment of anti-angiogenic resistant tumors

Although the treatment of tumors with anti-angiogenic therapies reveals clinical benefits, possible resistances or escape mechanisms ask for new solutions. In contrast to existing anti-angiogenic strategies, Chondramide inhibits angiogenesis via stress fiber solvation and the reduction of pro-migratory signaling cascades. This approach represents a broader strategy than established therapies targeting the VEGF signaling pathway and tackles a complete different target. Concluding, Chondramide might be effective where other treatments evoked resistances. To test this hypothesis, cell lines like the murine colon carcinoma cell line CT26, lymphoma EL4 or lewis lung carcinoma, that showed resistances over anti-VEGF therapies [94, 95], could be tested with regard to the anti-angiogenic potenial of Chondramide treatment in these systems.

4.4.2 Targeting both invasive migration modes to inhibit metastasis

Concerning metastasis, in the experimental setting tested in this work MDA-MB-231 cells show an amoeboid migration mode which can be inhibited with Chondramide. Other work shows that MDA-MB-231 cells are capable of migrating in a mesenchymal mode when embedded in collagen instead of matrigel [36]. However, when treated with protease inhibitors cells switch from the mesenchymal, Rac1 and protease dependent mode to the amoeboid mode which is protease independent [36]. This transition hampers the efficacy of protease inhibitors in the treatment of metastasis. Thus, protease inhibitors and Chondramide represent two classes of inhibitors interfering with opposing modes of invasion. Concluding, the combination of both would be interesting to examine whether invasion would be blocked completely or cells find another way to escape. Therefore, both migration modes could be tested *in vitro* in 3D matrices with single compared to combined application and *in vivo* metastasis could be investigated on combination therapy.

4.4.3 Improvement of tissue selectivity

Further, it did not escape our notice, that the approach of targeting the actin cytoskeleton requires special attention concerning tissue selectivity. The *in vivo* studies showed that there is a pharmacologically active window large enough for treating tumor angiogenesis or metastasis without acute toxicity in mice models. Still, for further development of Chondramide, this window would need further enlargement. This could be implemented by encapsulating or targeting the compound. E.g. Cytochalasin D was encapsulated in polyethylene liposomes which specifically accumulated in tumor tissue and inhibited tumor angiogenesis more effective than normal Cytochalasin D [96]. A similar approach would be possible for Chondramide which could be facilitated in collaboration with Prof. Dr. Ernst Wagner working on PEGylation drug delivery systems. Thereby, Chondramide could be encapsulated, tested *in vitro* on cell toxicity and functionality and, finally, *in vivo* studies should be performed investigating the effect on tumor growth and vascularization.

5: Summary

Tumor angiogenesis and cancer metastasis are crucial processes contributing to the progression of cancer. Both processes are based on cellular migration which involves high plasticity of the actin cytoskeleton. In the last centuries, actin targeting was thought to be too toxic, however, new actin binding substances are found and targeting strategies are further developed rising the interest in actin targeting again. Chondramide represents a new actin targeting compound that has not been tested for its suitability for cancer treatment so far. Isolated from the myxobacterium *Chondromyces crocatus*, Chondramides bind and polymerize actin in eukaryotic cells.

In this work, Chondramide was tested on its potency to inhibit angiogenesis and tumor metastasis. Further, the corresponding actin structures and pro-migratory signaling were analyzed to investigate the consequences of the actin binding compound.

In fact, we show that Chondramide inhibits major angiogenic processes such as endothelial cell proliferation, migration and tube formation in a lower nanomolar range. Intracellularly, Chondramide leads to an actin aggregation at stress fibers and reduces maturation of focal adhesions. At this signaling platform, the activation of Src is diminished under Chondramide treatment with the consequence of reduced RhoGTPase activation, thus, downregulating pro-migratory signals.

Concerning metastasis, Chondramide inhibits migration and invasion of the invasive cancer cell line MDA-MB-231 at nanomolar concentrations. We show that Chondramide abolishes the contractility of the cell which is achieved via two ways: first, an aggregation of stress fibers and, second, a force dependent negative feedback loop via Vav2 and Rho.

In vivo, Chondramide reduced the microvessel density in Chondramide treated tumors and the metastasis of cancer cells to the lung revealing a pharmacological active window without acute toxicity in two animal models.

Concluding, this work provides evidence for the feasibility of targeting actin with Chondramide to inhibit tumor angiogenesis and metastasis and gives first insights in the underlying intracellular processes in endothelial and metastatic cells. This work gives the basis for further development of actin binding compounds in low dose combination therapies or with specific targeting to treat tumor angiogenesis and metastasis.

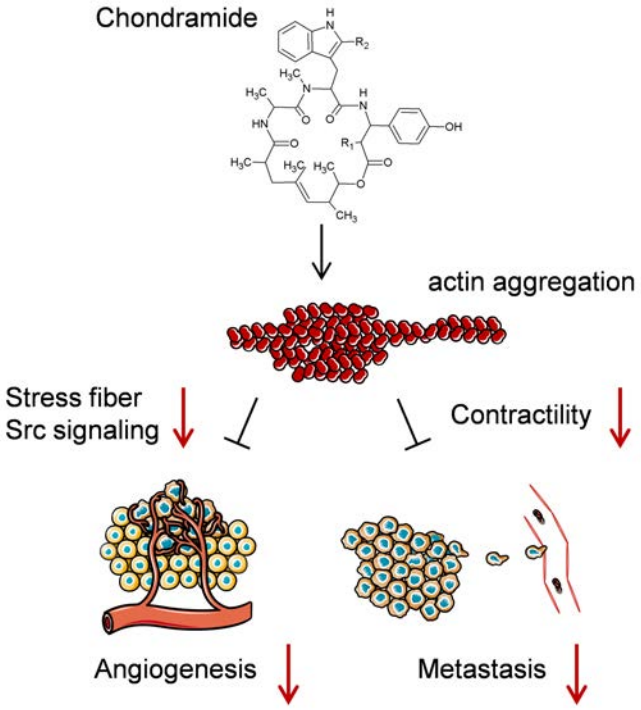

Figure 5.1: **Chondramide shows anti-angiogenic and anti-metastatic potency.** In endothelial cells, Chondramide induces stress fiber aggregation and inhibits the maturation of focal adhesions leading to reduced activity of Src as well as downstream Rho-GTPases Rac1 and Rho, thus, resulting in reduced angiogenesis. In invasive cancer cells, Chondramide reduces cellular contractility via stress fiber aggregation and dimished Rho activity, finally, reducing cancer cell metastasis.

Bibliography

[1] Jr. DeVita, V. T. and E. Chu. A history of cancer chemotherapy. *Cancer Res*, 68(21):8643–53, 2008.

[2] R. Fuerst and A. M. Vollmar. A new perspective on old drugs: non-mitotic actions of tubulin-binding drugs play a major role in cancer treatment. *Pharmazie*, 68(7):478–83, 2013.

[3] M. A. Jordan and L. Wilson. Microtubules as a target for anticancer drugs. *Nat Rev Cancer*, 4(4):253–65, 2004.

[4] T. D. Pollard and J. A. Cooper. Actin, a central player in cell shape and movement. *Science*, 326(5957):1208–12, 2009.

[5] L. J. Jones, R. Carballido-Lopez, and J. Errington. Control of cell shape in bacteria: helical, actin-like filaments in bacillus subtilis. *Cell*, 104(6):913–22, 2001.

[6] F. van den Ent, L. A. Amos, and J. Lowe. Prokaryotic origin of the actin cytoskeleton. *Nature*, 413(6851):39–44, 2001.

[7] G. P. 3rd Hemstreet, J. Rao, R. E. Hurst, R. B. Bonner, P. Waliszewski, H. B. Grossman, M. Liebert, and B. L. Bane. G-actin as a risk factor and modulatable endpoint for cancer chemoprevention trials. *J Cell Biochem Suppl*, 25:197–204, 1996.

[8] A. Algeciras-Schimnich, E. M. Pietras, B. C. Barnhart, P. Legembre, S. Vijayan, S. L. Holbeck, and M. E. Peter. Two cd95 tumor classes with different sensitivities to antitumor drugs. *Proc Natl Acad Sci U S A*, 100(20):11445–50, 2003.

[9] A. Loranger, B. Tuchweber, C. Gicquaud, S. St-Pierre, and M. G. Cote. Toxicity of peptides of amanita virosa mushrooms in mice. *Fundam Appl Toxicol*, 5(6 Pt 1):1144–52, 1985.

[10] V. R. Scott, R. Boehme, and T. R. Matthews. New class of antifungal agents: jasplakinolide, a cyclodepsipeptide from the marine sponge, jaspis species. *Antimicrob Agents Chemother*, 32(8):1154–7, 1988.

[11] C. G. dos Remedios, D. Chhabra, M. Kekic, I. V. Dedova, M. Tsubakihara, D. A. Berry, and N. J. Nosworthy. Actin binding proteins: regulation of cytoskeletal microfilaments. *Physiol Rev*, 83(2):433–73, 2003.

[12] G. M. Cragg and D. J. Newman. Plants as a source of anti-cancer agents. *J Ethnopharmacol*, 100(1-2):72–9, 2005.

[13] D. J. Newman and G. M. Cragg. Natural products as sources of new drugs over the last 25 years. *J Nat Prod*, 70(3):461–77, 2007.

[14] J. S. Allingham, V. A. Klenchin, and I. Rayment. Actin-targeting natural products: structures, properties and mechanisms of action. *Cell Mol Life Sci*, 63(18):2119–34, 2006.

[15] G. Fenteany and S. Zhu. Small-molecule inhibitors of actin dynamics and cell motility. *Curr Top Med Chem*, 3(6):593–616, 2003.

[16] T. Wieland and H. Faulstich. The action of phalloidin. *Curr Probl Clin Biochem*, 7:11–4, 1977.

[17] M. R. Bubb, A. M. Senderowicz, E. A. Sausville, K. L. Duncan, and E. D. Korn. Jasplakinolide, a cytotoxic natural product, induces actin polymerization and competitively inhibits the binding of phalloidin to f-actin. *J Biol Chem*, 269(21):14869–71, 1994.

[18] J. A. Cooper. Effects of cytochalasin and phalloidin on actin. *J Cell Biol*, 105(4):1473–8, 1987.

[19] I. Spector, N. R. Shochet, Y. Kashman, and A. Groweiss. Latrunculins: novel marine toxins that disrupt microfilament organization in cultured cells. *Science*, 219(4584):493–5, 1983.

[20] H. Reichenbach. Myxobacteria, producers of novel bioactive substances. *J Ind Microbiol Biotechnol*, 27(3):149–56, 2001.

[21] J. Diez, J. P. Martinez, J. Mestres, F. Sasse, R. Frank, and A. Meyerhans. Myxobacteria: natural pharmaceutical factories. *Microb Cell Fact*, 11:52, 2012.

[22] H. B. Bode and R. Muller. Analysis of myxobacterial secondary metabolism goes molecular. *J Ind Microbiol Biotechnol*, 33(7):577–88, 2006.

[23] K. J. Weissman and R. Muller. A brief tour of myxobacterial secondary metabolism. *Bioorg Med Chem*, 17(6):2121–36, 2009.

[24] B. Kunze, R. Jansen, F. Sasse, G. Hofle, and H. Reichenbach. Chondramides a approximately d, new antifungal and cytostatic depsipeptides from chondromyces crocatus (myxobacteria). production, physico-chemical and biological properties. *J Antibiot (Tokyo)*, 48(11):1262–6, 1995.

[25] R. Jansen, B. Kunze, H. Reichenbach, and G. Höfle. Chondramides a-d, new cytostatic and antifungal cyclodepsipeptides from chondromyces crocatus (myxobacteria): Isolation and structure elucidation. *Liebigs Ann.*, pages 285–290, 1996.

[26] F. Sasse, B. Kunze, T. M. Gronewold, and H. Reichenbach. The chondramides: cytostatic agents from myxobacteria acting on the actin cytoskeleton. *J Natl Cancer Inst*, 90(20):1559–63, 1998.

[27] L. G. Milroy, S. Rizzo, A. Calderon, B. Ellinger, S. Erdmann, J. Mondry, P. Verveer, P. Bastiaens, H. Waldmann, L. Dehmelt, and H. D. Arndt. Selective chemical imaging of static actin in live cells. *J Am Chem Soc*, 134(20):8480–6, 2012.

[28] J. Folkman. Angiogenesis: an organizing principle for drug discovery? *Nat Rev Drug Discov*, 6(4):273–86, 2007.

[29] K. J. Bayless and G. A. Johnson. Role of the cytoskeleton in formation and maintenance of angiogenic sprouts. *J Vasc Res*, 48(5):369–85, 2011.

[30] I. J. Fidler. The pathogenesis of cancer metastasis: the 'seed and soil' hypothesis revisited. *Nat Rev Cancer*, 3(6):453–8, 2003.

[31] C. L. Chaffer and R. A. Weinberg. A perspective on cancer cell metastasis. *Science*, 331(6024):1559–64, 2011.

[32] L. Lamalice, F. Le Boeuf, and J. Huot. Endothelial cell migration during angiogenesis. *Circ Res*, 100(6):782–94, 2007.

[33] T. J. Mitchison and L. P. Cramer. Actin-based cell motility and cell locomotion. *Cell*, 84(3):371–9, 1996.

[34] M. F. Olson and E. Sahai. The actin cytoskeleton in cancer cell motility. *Clin Exp Metastasis*, 26(4):273–87, 2009.

[35] E. Sahai and C. J. Marshall. Differing modes of tumour cell invasion have distinct requirements for rho/rock signalling and extracellular proteolysis. *Nat Cell Biol*, 5(8):711–9, 2003.

[36] K. Wolf, I. Mazo, H. Leung, K. Engelke, U. H. von Andrian, E. I. Deryugina, A. Y. Strongin, E. B. Brocker, and P. Friedl. Compensation mechanism in tumor cell migration: mesenchymal-amoeboid transition after blocking of pericellular proteolysis. *J Cell Biol*, 160(2):267–77, 2003.

[37] E. Sahai. Mechanisms of cancer cell invasion. *Curr Opin Genet Dev*, 15(1):87–96, 2005.

[38] A. J. Ridley. Rho gtpases and cell migration. *J Cell Sci*, 114(Pt 15):2713–22, 2001.

[39] A. L. Bishop and A. Hall. Rho gtpases and their effector proteins. *Biochem J*, 348 Pt 2:241–55, 2000.

[40] K. Rottner and T. E. Stradal. Actin dynamics and turnover in cell motility. *Curr Opin Cell Biol*, 23(5):569–78, 2011.

[41] H. Yamaguchi and J. Condeelis. Regulation of the actin cytoskeleton in cancer cell migration and invasion. *Biochim Biophys Acta*, 1773(5):642–52, 2007.

[42] A. A. Schmitz, E. E. Govek, B. Bottner, and L. Van Aelst. Rho gtpases: signaling, migration, and invasion. *Exp Cell Res*, 261(1):1–12, 2000.

[43] G. B. Mills and W. H. Moolenaar. The emerging role of lysophosphatidic acid in cancer. *Nat Rev Cancer*, 3(8):582–91, 2003.

[44] S. K. Mitra and D. D. Schlaepfer. Integrin-regulated fak-src signaling in normal and cancer cells. *Curr Opin Cell Biol*, 18(5):516–23, 2006.

[45] S. Huveneers and E. H. Danen. Adhesion signaling - crosstalk between integrins, src and rho. *J Cell Sci*, 122(Pt 8):1059–69, 2009.

[46] K. A. DeMali, K. Wennerberg, and K. Burridge. Integrin signaling to the actin cytoskeleton. *Curr Opin Cell Biol*, 15(5):572–82, 2003.

[47] F. Peng, B. Zhang, A. J. Ingram, B. Gao, Y. Zhang, and J. C. Krepinsky. Mechanical stretch-induced rhoa activation is mediated by the rhogef vav2 in mesangial cells. *Cell Signal*, 22(1):34–40, 2010.

[48] E. C. Lessey, C. Guilluy, and K. Burridge. From mechanical force to rhoa activation. *Biochemistry*, 51(38):7420–32, 2012.

[49] J. Herrmann, S. Huttel, and R. Muller. Discovery and biological activity of new chondramides from chondromyces sp. *Chembiochem*, 14(13):1573–80, 2013.

[50] E. W. Ades, F. J. Candal, R. A. Swerlick, V. G. George, S. Summers, D. C. Bosse, and T. J. Lawley. Hmec-1: establishment of an immortalized human microvascular endothelial cell line. *J Invest Dermatol*, 99(6):683–90, 1992.

[51] D. Bouis, G. A. Hospers, C. Meijer, G. Molema, and N. H. Mulder. Endothelium in vitro: a review of human vascular endothelial cell lines for blood vessel-related research. *Angiogenesis*, 4(2):91–102, 2001.

[52] R. Cailleau, R. Young, M. Olive, and Jr. Reeves, W. J. Breast tumor cell lines from pleural effusions. *J Natl Cancer Inst*, 53(3):661–74, 1974.

[53] R. Cailleau, M. Olive, and Q. V. Cruciger. Long-term human breast carcinoma cell lines of metastatic origin: preliminary characterization. *In Vitro*, 14(11):911–5, 1978.

[54] M. Lacroix and G. Leclercq. Relevance of breast cancer cell lines as models for breast tumours: an update. *Breast Cancer Res Treat*, 83(3):249–89, 2004.

[55] I. Nicoletti, G. Migliorati, M. C. Pagliacci, F. Grignani, and C. Riccardi. A rapid and simple method for measuring thymocyte apoptosis by propidium iodide staining and flow cytometry. *J Immunol Methods*, 139(2):271–9, 1991.

[56] R. Poincloux, O. Collin, F. Lizarraga, M. Romao, M. Debray, M. Piel, and P. Chavrier. Contractility of the cell rear drives invasion of breast tumor cells in 3d matrigel. *Proc Natl Acad Sci U S A*, 108(5):1943–8, 2011.

[57] M. M. Bradford. A rapid and sensitive method for the quantitation of microgram quantities of protein utilizing the principle of protein-dye binding. *Anal Biochem*, 72:248–54, 1976.

[58] Sambrook. J and Russell DW. *Molecular Cloning–Laboratory manuals.*, volume 3. Cold Spring Harbor Laboratory Press, Cold Spirng Harbor, New York, 3rd edition, 2001.

[59] J. A. Johnston, C. L. Ward, and R. R. Kopito. Aggresomes: a cellular response to misfolded proteins. *J Cell Biol*, 143(7):1883–98, 1998.

[60] S. Kazami, T. Usui, and H. Osada. Actin stress fiber retraction and aggresome formation is a common cellular response to actin toxins. *Biosci Biotechnol Biochem*, 75(9):1853–5, 2011.

[61] F. Foerster, S. Braig, C. Moser, R. Kubisch, J. Busse, E. Wagner, E. Schmoeckel, D. Mayr, S. Schmitt, S. Huettel, H. Zischka, R Mueller, and A.M. Vollmar. Targeting the actin cytoskeleton: selective anti-tumor action via trapping pkcepsilon. *submitted*, 2014.

[62] C. J. Aslakson and F. R. Miller. Selective events in the metastatic process defined by analysis of the sequential dissemination of subpopulations of a mouse mammary tumor. *Cancer Res*, 52(6):1399–405, 1992.

[63] J. Li and G. G. Sahagian. Demonstration of tumor suppression by mannose 6-phosphate/insulin-like growth factor 2 receptor. *Oncogene*, 23(58):9359–68, 2004.

[64] J. Yang, S. A. Mani, J. L. Donaher, S. Ramaswamy, R. A. Itzykson, C. Come, P. Savagner, I. Gitelman, A. Richardson, and R. A. Weinberg. Twist, a master regulator of morphogenesis, plays an essential role in tumor metastasis. *Cell*, 117(7):927–39, 2004.

[65] L. Schreiner. *Innovative cancer therapeutics based on polymers or biogenic drugs evaluated in murine tumor models.* PhD thesis, LMU München, 2013.

[66] R. J. Bloom, J. P. George, A. Celedon, S. X. Sun, and D. Wirtz. Mapping local matrix remodeling induced by a migrating tumor cell using three-dimensional multiple-particle tracking. *Biophys J*, 95(8):4077–88, 2008.

[67] T. Wieland and H. Faulstich. Amatoxins, phallotoxins, phallolysin, and antamanide: the biologically active components of poisonous amanita mushrooms. *CRC Crit Rev Biochem*, 5(3):185–260, 1978.

[68] L. Thoenes and M. Gunther. Novel approaches in anti-angiogenic treatment targeting endothelial f-actin: a new anti-angiogenic strategy? *Curr Opin Mol Ther*, 10(6):579–90, 2008.

[69] P. Mabeta and M. S. Pepper. A comparative study on the anti-angiogenic effects of dna-damaging and cytoskeletal-disrupting agents. *Angiogenesis*, 12(1):81–90, 2009.

[70] G. Melkonian, N. Munoz, J. Chung, C. Tong, R. Marr, and P. Talbot. Capillary plexus development in the day five to day six chick chorioallantoic membrane is inhibited by cytochalasin d and suramin. *J Exp Zool*, 292(3):241–54, 2002.

[71] K. A. El Sayed, D. T. Youssef, and D. Marchetti. Bioactive natural and semisynthetic latrunculins. *J Nat Prod*, 69(2):219–23, 2006.

[72] K. Schweikart, L. Guo, Z. Shuler, R. Abrams, E. T. Chiao, K. L. Kolaja, and M. Davis. The effects of jaspamide on human cardiomyocyte function and cardiac ion channel activity. *Toxicol In Vitro*, 27(2):745–51, 2013.

[73] R. Garcia-Mata, Z. Bebok, E. J. Sorscher, and E. S. Sztul. Characterization and dynamics of aggresome formation by a cytosolic gfp-chimera. *J Cell Biol*, 146(6):1239–54, 1999.

[74] F. Lazaro-Dieguez, C. Aguado, E. Mato, Y. Sanchez-Ruiz, I. Esteban, J. Alberch, E. Knecht, and G. Egea. Dynamics of an f-actin aggresome generated by the actin-stabilizing toxin jasplakinolide. *J Cell Sci*, 121(Pt 9):1415–25, 2008.

[75] H. Wolfenson, Y. I. Henis, B. Geiger, and A. D. Bershadsky. The heel and toe of the cell's foot: a multifaceted approach for understanding the structure and dynamics of focal adhesions. *Cell Motil Cytoskeleton*, 66(11):1017–29, 2009.

[76] Jr. Roskoski, R. Src kinase regulation by phosphorylation and dephosphorylation. *Biochem Biophys Res Commun*, 331(1):1–14, 2005.

[77] D. D. Schlaepfer, C. R. Hauck, and D. J. Sieg. Signaling through focal adhesion kinase. *Prog Biophys Mol Biol*, 71(3-4):435–78, 1999.

[78] V. J. Fincham, M. Unlu, V. G. Brunton, J. D. Pitts, J. A. Wyke, and M. C. Frame. Translocation of src kinase to the cell periphery is mediated by the actin cytoskeleton under the control of the rho family of small g proteins. *J Cell Biol*, 135(6 Pt 1):1551–64, 1996.

[79] P. Timpson, G. E. Jones, M. C. Frame, and V. G. Brunton. Coordination of cell polarization and migration by the rho family gtpases requires src tyrosine kinase activity. *Curr Biol*, 11(23):1836–46, 2001.

[80] K. Yoshioka, S. Nakamori, and K. Itoh. Overexpression of small gtp-binding protein rhoa promotes invasion of tumor cells. *Cancer Res*, 59(8):2004–10, 1999.

[81] D. Rosel, J. Brabek, O. Tolde, C. T. Mierke, D. P. Zitterbart, C. Raupach, K. Bicanova, P. Kollmannsberger, D. Pankova, P. Vesely, P. Folk, and B. Fabry. Up-regulation of rho/rock signaling in sarcoma cells drives invasion and increased generation of protrusive forces. *Mol Cancer Res*, 6(9):1410–20, 2008.

[82] P. R. Molli, L. Adam, and R. Kumar. Therapeutic imc-c225 antibody inhibits breast cancer cell invasiveness via vav2-dependent activation of rhoa gtpase. *Clin Cancer Res*, 14(19):6161–70, 2008.

[83] B. Escudier, J. Bellmunt, S. Negrier, E. Bajetta, B. Melichar, S. Bracarda, A. Ravaud, S. Golding, S. Jethwa, and V. Sneller. Phase iii trial of bevacizumab plus interferon alfa-2a in patients with metastatic renal cell carcinoma (avoren): final analysis of overall survival. *J Clin Oncol*, 28(13):2144–50, 2010.

[84] A. J. Montero, M. Escobar, G. Lopes, S. Gluck, and C. Vogel. Bevacizumab in the treatment of metastatic breast cancer: friend or foe? *Curr Oncol Rep*, 14(1):1–11, 2012.

[85] C. J. Allegra, G. Yothers, M. J. O'Connell, S. Sharif, N. J. Petrelli, L. H. Colangelo, J. N. Atkins, T. E. Seay, L. Fehrenbacher, R. M. Goldberg, S. O'Reilly, L. Chu, C. A. Azar, S. Lopa, and N. Wolmark. Phase iii trial assessing bevacizumab in stages ii and iii carcinoma of the colon: results of nsabp protocol c-08. *J Clin Oncol*, 29(1):11–6, 2011.

[86] S. Giuliano and G. Pages. Mechanisms of resistance to anti-angiogenesis therapies. *Biochimie*, 95(6):1110–9, 2013.

[87] A. Orimo, P. B. Gupta, D. C. Sgroi, F. Arenzana-Seisdedos, T. Delaunay, R. Naeem, V. J. Carey, A. L. Richardson, and R. A. Weinberg. Stromal fibroblasts present in invasive human breast carcinomas promote tumor growth and angiogenesis through elevated sdf-1/cxcl12 secretion. *Cell*, 121(3):335–48, 2005.

[88] O. Casanovas, D. J. Hicklin, G. Bergers, and D. Hanahan. Drug resistance by evasion of antiangiogenic targeting of vegf signaling in late-stage pancreatic islet tumors. *Cancer Cell*, 8(4):299–309, 2005.

[89] Y. Crawford, I. Kasman, L. Yu, C. Zhong, X. Wu, Z. Modrusan, J. Kaminker, and N. Ferrara. Pdgf-c mediates the angiogenic and tumorigenic properties of fibroblasts associated with tumors refractory to anti-vegf treatment. *Cancer Cell*, 15(1):21–34, 2009.

[90] G. Bergers and D. Hanahan. Modes of resistance to anti-angiogenic therapy. *Nat Rev Cancer*, 8(8):592–603, 2008.

[91] M. Paez-Ribes, E. Allen, J. Hudock, T. Takeda, H. Okuyama, F. Vinals, M. Inoue, G. Bergers, D. Hanahan, and O. Casanovas. Antiangiogenic therapy elicits malignant progression of tumors to increased local invasion and distant metastasis. *Cancer Cell*, 15(3):220–31, 2009.

[92] R. M. Zuniga, R. Torcuator, R. Jain, J. Anderson, T. Doyle, S. Ellika, L. Schultz, and T. Mikkelsen. Efficacy, safety and patterns of response and recurrence in patients with recurrent high-grade gliomas treated with bevacizumab plus irinotecan. *J Neurooncol*, 91(3):329–36, 2009.

[93] F. Shojaei, B. H. Simmons, J. H. Lee, P. B. Lappin, and J. G. Christensen. Hgf/c-met pathway is one of the mediators of sunitinib-induced tumor cell type-dependent metastasis. *Cancer Lett*, 320(1):48–55, 2012.

[94] C. Fischer, B. Jonckx, M. Mazzone, S. Zacchigna, S. Loges, L. Pattarini, E. Chorianopoulos, L. Liesenborghs, M. Koch, M. De Mol, M. Autiero, S. Wyns, S. Plaisance, L. Moons, N. van Rooijen, M. Giacca, J. M. Stassen, M. Dewerchin, D. Collen, and P. Carmeliet. Anti-plgf inhibits growth of vegf(r)-inhibitor-resistant tumors without affecting healthy vessels. *Cell*, 131(3):463–75, 2007.

[95] F. Shojaei, X. Wu, A. K. Malik, C. Zhong, M. E. Baldwin, S. Schanz, G. Fuh, H. P. Gerber, and N. Ferrara. Tumor refractoriness to anti-vegf treatment is mediated by cd11b+gr1+ myeloid cells. *Nat Biotechnol*, 25(8):911–20, 2007.

[96] F. Y. Huang, W. L. Mei, Y. N. Li, G. H. Tan, H. F. Dai, J. L. Guo, H. Wang, Y. H. Huang, H. G. Zhao, S. L. Zhou, L. Li, and Y. Y. Lin. The antitumour activities induced by pegylated liposomal cytochalasin d in murine models. *Eur J Cancer*, 48(14):2260–9, 2012.

Appendix

6.1 Abbreviations

Table 6.1: **List of abbreviations**

Abbreviation	**Full name**
BSA	Bovine serum albumin
CAM	Chorioallantoic membrane
Ch	Chondramide
Cyto	Cytochalasin
DMEM	Dulbecco's Modified Eagle Medium
DMSO	Dimethylsulfoxide
EC	Endothelial cell
ECGM	Endothelial cell growth medium
ECL	Enhanced chemoluminescence
ECM	Extracellular matrix
EDTA	Ethylenediaminetetraacetic acid
EGTA	Ethylene glycol tetraacetic acid
EGF	Epidermal growth factor
EGF-R	Epidermal growth factor receptor
FACS	Fluorescence activated cell sorter
F-actin	Fibrilous actin
FAK	Focal adhesion kinase
FCS	Fetal calf serum
GAPDH	Glyceraldehyde 3-phosphate dehydrogenase
GEF	Guanine nucleotide exchange factor
HMEC	Human microvascular endothelial cell
HUVEC	Human umbilical vein endothelial cell
Jk	Jasplakinolide
MLC	Myosin light chain
MTOC	Microtubule organizing center
PBS	Phosphate buffered saline
PDGF	Platelet derived growth factor
p-FA	Para-formaldehyde
PIV	Particle image velocimetry
PMSF	Phenylmethylsulfonyl fluoride
SDS	Sodium dodecyl sulfate
VEGF	Vascular endothelial growth factor

6.2 Publications

6.2.1 Articles

M. H. Menhofer, D. Bartel, R. Kubisch, J. Busse, E. Wagner, R. Müller, A. M. Vollmar, S. Zahler; *In vitro and in vivo characterization of the actin polymerizing compound Chondramide as angiogenic inhibitor.*; submitted

M. H. Menhofer, R. Kubisch, L. Schreiner, M. Zorn, F. Förster, R. Müller, J. O. Rädler, E. Wagner, A. M. Vollmar, S. Zahler; *The actin targeting compound Chondramide inhibits breast cancer metastasis via reduction of cellular contractility.*; submitted

6.2.2 Oral presentations

M. H. Menhofer, R. Kubisch, L. Schreiner, R. Müller, E. Wagner, A. M. Vollmar, S. Zahler; *Chondramide reduces angiogenesis and metastasis via affecting stress fibers and Rho activity*; 4th FOR 1406 Meeting, July 16-18, 2013, Saarbrücken, Germany

M. H. Menhofer, R. Kubisch, L. Schreiner, R. Müller, E. Wagner, A. M. Vollmar, S. Zahler; *Chondramide inhibits angiogenesis and metastasis*; Retreat Graduate School LSM, May 5-9, 2013, Starnberg, Germany

M. H. Menhofer, R. Kubisch, L. Schreiner, R. Müller, E. Wagner, A. M. Vollmar, S. Zahler; *Chondramide shows anti-angiogenic and anti-metastatic potency*; 3rd FOR 1406 Meeting, September 16-18, 2012, Starnberg, Germany

M. H. Menhofer, R. Müller, A. M. Vollmar, S. Zahler; *Chondramide A – a potent agent to inhibit cell migration and angiogenesis?*; 2nd FOR 1406 Meeting, October 26, 2011, Munich, Germany

6.2.3 Poster presentations

M. H. Menhofer, R. Kubisch, L. Schreiner, R. Müller, E. Wagner, A. M. Vollmar, S. Zahler; *The myxobacterial compound chondramide shows anti-angiogenic and anti-migratory potency*; 1st European Conference on Natural Products: Research and Applications, September 22-25, 2013, Frankfurt, Germany

M. H. Menhofer, V. Kretschmann, R. Müller, R. Fürst, A. M. Vollmar, S. Zahler; *The myxobacterial compound chondramide shows anti-angiogenic and anti-migratory potency*; Natural Anticancer Drugs, June 30 – July 4, 2012, Olomouc, Czech Republic
Honored with the 'Student Poster Award'

M. H. Menhofer, R. Müller, A. M. Vollmar, S. Zahler; *Chondramide A – a potent agent to inhibit cell migration and angiogenesis?*; Retreat Graduate School LSM, September 13 and 18, 2011, Schliersee, Germany

6.3 Danksagung

Mein allergrößter Dank geht an Frau Prof. Dr. Vollmar und Herrn Prof. Dr. Zahler. Ich danke Ihnen ganz herzlich, dass ich meine Doktorarbeit bei Ihnen anfertigen konnte. In den drei Jahren, die ich bei Ihnen arbeiten konnte, habe ich zum einen methodisch und wissenschaftlich viel gelernt, zum anderen aber vor allem auch menschlich viel mitnehmen können. Danke dafür!

Ein besonders großer Dank geht an Herrn Zahler. Vielen Dank für die offene Tür bei allen Fragen und zu jeder Zeit. Vielen Dank für Ihr Vertrauen und die Selbständigkeit die Sie mir für die Anfertigung der Arbeit überließen, sowie Ihre humorvolle Art.

Frau Vollmar möchte ich speziell für die gute Führung Ihres Lehrstuhls danken, von der ich als Mitarbeiter profitieren konnte. Die gute Strukturierung ermöglicht eine hervorragende Betreuung und ein effizientes Arbeiten. Zudem lassen Sie Ihre Mitarbeiter Ihre Wertschätzung wissen, was sich unglaublich positiv auf das Arbeitsklima auswirkt.

Herrn Prof. Wagner und Herrn PD Michalakis danke ich ganz herzlich, dass Sie sich bereit erklärt haben als Dritt- beziehungsweise Viertprüfer zu fungieren, sowie Herrn Prof. Frieß und Herrn Prof. Paintner als Fünft- und Sechstprüfer. Vielen Dank für den zusätzlichen Zeitaufwand.

Ein großer Dank geht auch an Matthias Zorn und Herrn Prof. Dr. Rädler für die gute Zusammenarbeit im Metastasierungsprojekt.

Ich bedanke mich auch sehr, meine Arbeit im Rahmen der Forschergruppe FOR1406 angefertigt haben zu können, sowie in der Graduierten Schule 'Graduate School Life Science Munich' der LMU teilnehmen zu dürfen. Der Austausch mit angrenzenden Forschergruppen, die Reisen und Vorträge haben meine Zeit als Doktrorandin sehr bereichert.